The Braidwood Experiment: Project Summary

This document describes plans for a two-location neutrino oscillation experiment at the Braidwood Nuclear Power Station in Illinois. The goal of the experiment is to measure θ_{13}, the last unmeasured angle of the neutrino mixing matrix, with a sensitivity of $\sin^2 2\theta_{13} \sim 0.01$.

Recent years have seen enormous progress in the physics of neutrino mixing, but several critical questions remain: What is the value of θ_{13}, the last unmeasured mixing angle in the neutrino mixing matrix? What is the mass hierarchy? (i.e., what is the sign of $m_1^2 - m_3^2$). Do neutrino oscillations violate CP symmetry? Why are the quark and neutrino mixing matrices so different? The value of θ_{13} is central to each of these questions. Its value sets the scale for experiments needed to resolve the mass hierarchy and to search for CP violation. In addition, the size of θ_{13} with respect to the other mixing angles may give insights into the orgin of these angles and source of neutrino mass. Reactor experiments hold the promise of unambiguously determining the θ_{13} mixing angle.

The Braidwood Experiment will be sensitive to $\sin^2 2\theta_{13}$ at the level of 0.01. The APS Multidisciplinary Study on the Future of Neutrino Physics identified a reactor experiment with this precision as one of the highest priorities in the field. The Braidwood site is ideal for the θ_{13} measurement, and also has the unique potential to make a precise measurement of the weak mixing angle, $\sin^2 \theta_W$. The flat overburden at Braidwood allows for a design with great flexibility, redundancy, and cross checks. The baseline design has four 65 fiducial tonne detectors, two at 200m and two at 1500m (horizontal distance) from the reactor. The detectors can be moved between locations to provide cross calibration and to respond to physics results. For example, moving one or two of the near detectors to the far location could provide even better sensitivity to $\sin^2 2\theta_{13}$ if the mixing angle is found to be small.

The Exelon Corporation, which owns the Braidwood site, has encouraged us to move toward submission of a full proposal as soon as possible, and has provided a letter of support that is included in this proposal. In December 2004, we used a 3rd party contractor to drill bore holes to the full experimental depth at the near and far shaft locations, both on Exelon property, as a first step in finalizing the civil construction design. With this cooperation, a reactor experiment is a timely and cost-effective way to perform this measurement: the neutrino source exists and the required detectors are of modest size and complexity.

Contents

Project Description

1 Introduction

1.1 Status of Neutrino Oscillations and Next Steps

The last ten years have been a remarkable period in neutrino physics. Oscillations between different flavors of neutrinos have been established with two distinct mass differences.[1] The observations are elegantly described by a picture in which the neutrino flavor eigenstates (ν_e, ν_μ, and ν_τ) are mixtures of mass eigenstates (ν_1, ν_2, and ν_3), analogous to mixing in the quark sector. This mixing is described by a 3×3 unitary matrix known as the MNSP matrix:

$$\begin{pmatrix} U_{e1} & U_{e2} & U_{e3} \\ U_{\mu 1} & U_{\mu 2} & U_{\mu 3} \\ U_{\tau 1} & U_{\tau 2} & U_{\tau 3} \end{pmatrix} = \begin{pmatrix} \cos\theta_{12} & \sin\theta_{12} & 0 \\ -\sin\theta_{12} & \cos\theta_{12} & 0 \\ 0 & 0 & 1 \end{pmatrix} \begin{pmatrix} \cos\theta_{13} & 0 & e^{-i\delta}\sin\theta_{13} \\ 0 & 1 & 0 \\ -e^{-i\delta}\sin\theta_{13} & 0 & \cos\theta_{13} \end{pmatrix} \begin{pmatrix} 1 & 0 & 0 \\ 0 & \cos\theta_{23} & \sin\theta_{23} \\ 0 & -\sin\theta_{23} & \cos\theta_{23} \end{pmatrix}.$$

As shown, this matrix is often written in terms of 3 Euler rotations (θ_{12}, θ_{13}, and θ_{23}) and a CP violating phase (δ_{CP}). The (12) parameters refer to solar neutrino oscillations, and the (23) parameters refer to atmospheric neutrino oscillations.

Several important questions related to the mixing of neutrino species still remain and define the goals for the future experimental program. These questions include: What is the value of θ_{13}, the last unmeasured mixing angle in the neutrino mixing matrix? What is the mass hierarchy? (i.e., what is the sign of $m_1^2 - m_3^2$). Do neutrino oscillations violate CP symmetry? Why are the quark and neutrino mixing matrices so different?

The value of θ_{13} is central to each of these questions. Its value sets the scale for experiments needed to resolve the mass hierarchy and to search for CP violation. In addition, the size of θ_{13} with respect to the other mixing angles may give insights into the orgin of these angles and the source of neutrino mass [1]. Reactor experiments hold the promise of determining the θ_{13} mixing angle unambiguously. A reactor experiment is also a timely and cost effective way to perform this measurement: the neutrino source exists and the required detectors can be of modest size and complexity.

This proposal requests funding to complete the design and engineering for a two location neutrino oscillation experiment at the Braidwood Nuclear Power Station in Illinois. The proposed experiment will be sensitive to $\sin^2 2\theta_{13} = 0.01$ at the 90% confidence level. This precision is necessary, as outlined in the APS Neutrino Study, both for furthering the knowledge of oscillation phenomena, and for making future plans to study the mass hierarchy and CP violation in the neutrino sector.

The Braidwood site is ideal for the θ_{13} measurement, and also has the unique potential to make a precise measurement of the weak mixing angle, $\sin^2\theta_W$. In addition, the flat overburden available at Braidwood allows for a design with great flexibility, redundancy, and cross checks. The baseline design has four 65 fiducial ton detectors, two at 200m and two at 1500m (horizontal distance) from the reactor. The detectors can be moved between these locations to provide cross calibration and

[1] The LSND experiment has observed an oscillation signal with a third Δm^2 value. If this observation is confirmed, it will require a modification of the picture described here.

to respond to physics results. For example, moving a far detector to the near site for 10% of the time can provide a check of the relative efficiency to the 0.3% level, and moving one or two of the near detectors to the far location could provide even better sensitivity to $\sin^2 2\theta_{13}$ if the mixing angle is found to be small.

The Exelon Corporation, which owns the Braidwood plant, has been extremely cooperative in our initial studies, and have committed to work with us as we prepare a proposal for the experiment. As described in their letter of support for this proposal, they fully support our plans for the Braidwood Experiment. In the fall of 2004, Exelon and The University of Chicago concluded an agreement to drill of bore holes to full depth at the near and far sites; this work was completed in December 2004.

Following a brief discussion of the physics impact of a reactor experiment, Section 2 describes the strategy of the Braidwood Experiment and outstanding questions. Section 3 includes our preliminary cost estimate for the experiment, and the proposed engineering and R&D required to complete the design of the experiment. Section 4 reviews the potential of this experiment to make a precision measurement of $\overline{\nu}_e$ elastic scattering.

1.2 Reactor experiment: Contributions and comparisons

As introduced above, neutrino oscillations are described by six physics parameters: $\theta_{13}, \theta_{12}, \theta_{23}$, Δm^2_{12}, Δm^2_{23}, and the CP violation phase, δ. In addition, a full description also requires knowing the hierarchy of mass state 3 relative to 1 and 2, *i.e.* the sign of Δm^2_{23}. Of the six parameters, $\theta_{12}, \sin^2 2\theta_{23}, \Delta m^2_{12}$, and Δm^2_{23} are fairly well known and will be addressed with greater precision through the current and planned long-baseline programs (SuperK, Minos, T2K, Nova and CNGS). This leaves for determination θ_{13}, δ, the value of θ_{23}, and the mass hierarchy. Reactor experiments measure θ_{13} directly and are necessary to determine θ_{23}, which are prime ingredients needed to move toward determining δ_{CP} and the mass hierarchy.

The leading order dependence of the oscillation probability for reactor and long-baseline measurements is given by

$$P_R = 1 - P(\overline{\nu}_e \to \overline{\nu}_e) \simeq \sin^2 2\theta_{13} \sin^2\left(1.27\Delta m^2_{31} L/E\right) + \text{negligible corrections}$$

$$\begin{aligned} P_{LB} = P(\nu_\mu \to \nu_e) &\simeq \sin^2 2\theta_{13} \sin^2\theta_{23} \sin^2\left(1.27\Delta m^2_{31} L/E\right) + \\ &+ \text{significant corrections}(\delta_{CP}, sign(\Delta m^2_{13})) \end{aligned}$$

The higher order corrections for the reactor probability are quite small for the Braidwood experimental layout so a measurement of P_R directly constrains the mixing parameter θ_{13}. On the other hand, the full expression for the long-baseline probability introduces many degeneracies and correlations between the physics parameters θ_{23} and δ_{CP}, plus the mass hierarchy through matter effects even before experimental uncertainties are taken into account [2, 3, 4, 5]. Therefore, a measurement of P_{LB} corresponds to sizeable regions in the physics parameter space. For this reason, a reactor experiment is ideal for determining θ_{13} and, in combination with the off-axis data, θ_{23}.

As will be shown in the following sections, the Braidwood experiment will have a sensitivity equal to or better than $\sin^2 2\theta_{13} = 0.01$ at the 90% CL. For most of parameter space, this experiment is better at constraining the value of $\sin^2 2\theta_{13}$ than either the T2K or Nova experiments even with

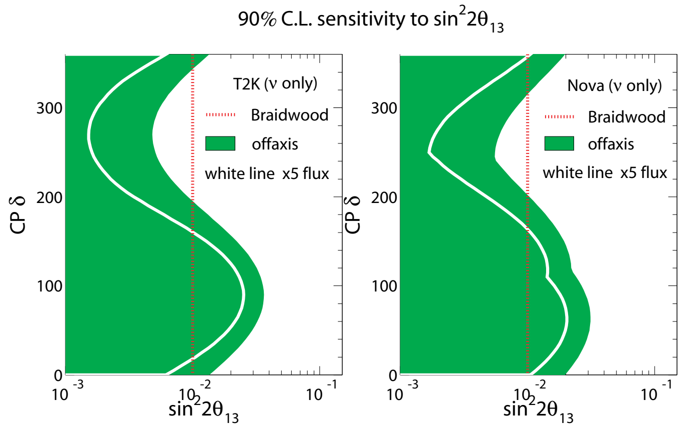

Figure 1: 90% C.L. upper limit regions for various oscillation measurements for an underlying null oscillation scenario where $\sin^2 2\theta_{13} = 0$ ($\sin^2 2\theta_{23} = 0.95 \pm 0.01$ and $\Delta m^2 = 2.5 \pm 0.01 \times 10^{-3}$ eV^2). The left (right) plot is for the T2K (Nova) long-baseline experiment. The vertical dotted line in each plot corresponds to the 90% C.L. upper limit from a Braidwood reactor measurement. The shaded region (white curve) is the 90% C.L. allowed region for the long-baseline experiments for a three year neutrino-only run with nominal ($\times 5$) beam rate. (from Ref. [7])

the intensity upgrades being proposed as shown in Fig. 1. The size of θ_{13} sets the scale for which the off-axis experiments can start to probe CP violation and the mass hierarchy. A combination of T2K and Nova will start to give some information about these effects if $\sin^2 2\theta_{13} > 0.05$ and, as shown in Fig. 2, with enhanced beam rates will have complete coverage if $\sin^2 2\theta_{13} > 0.01$. Thus, an unambiguous determination of $\sin^2 2\theta_{13}$ at the 0.01 level from a reactor experiment is a crucial ingredient in planning the strategy for a neutrino oscillation program, as well as for accessing the phenomenology of neutrino mixing.

Several groups around the world have also been investigating reactor neutrino oscillation experiments including experiments at Daya Bay in China, Diablo Canyon in California, the CHOOZ reactor in France (Double CHOOZ), the Kashiwazaki reactor in Japan, and Angra in Brazil. At this time, details of these possibilities are preliminary except for the Double CHOOZ experiment which has submitted a Letter of Intent to the French government [6]. In comparison to all of these possibilities, the Braidwood experiment has better or comparable sensitivity with better redundancy and cross checks, and has a clear upgrade path. Specifically, Braidwood has three times better sensitivity than Double CHOOZ at a cost which is about three times higher. It is clear that reaching the sensitivity goal, as outlined in the recent APS Neutrino Study, of $\sin^2 2\theta_{13} \approx 0.01$ in a robust manner will require an experiment of the size and design of Braidwood that includes these redundancies and cross checks.

2 Strategy to reach sensitivity of $\sin^2 2\theta_{13} \sim 0.01$

In this section, we describe important features of our strategy to reach a sensitivity of $\sin^2 2\theta_{13} \sim 0.01$. Areas requiring additional study and R&D are discussed in Section 2.6.

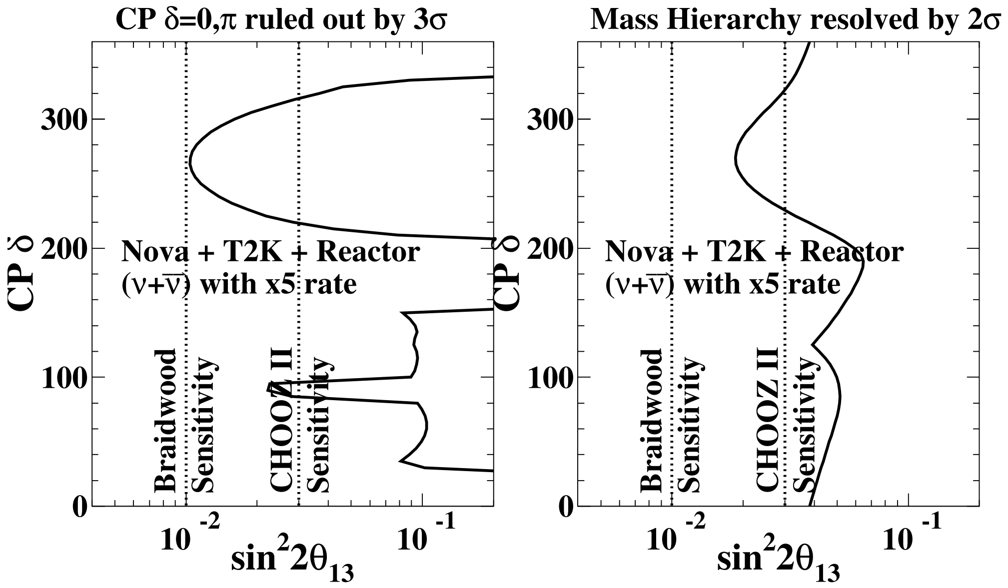

Figure 2: Regions of true CP phase δ versus true $\sin^2 2\theta_{13}$ where: (Left) a combination of data can observe CP violation at the three standard deviation level and (Right) the combination of data can resolve the mass hierarchy at the two standard deviation level. The assumed data is a combination of the T2K, Noνa and Braidwood reactor experiments. For both plots, the T2K and Nova data sets are assumed to be with upgraded beam fluxes ($\times 5$ the nominal rate) as would be expected with upgrades or a new proton driver. The vertical line in both plots represent the 90% C.L. $\sin^2 2\theta_{13}$ sensitivities for the Braidwood experiment. For these plots, $\Delta m^2 = 2.5^{-3}$ eV^2. (from Ref. [7])

2.1 Overview of Braidwood Experiment

The Braidwood Experiment is designed to reach a sensitivity of $\sin^2 2\theta_{13} \sim 0.01$, with the capability to push below this limit in the longer term should the mixing angle turn out to be small. Key features of the design include: a high power reactor, multiple identical near and far detector modules with large enough fiducial mass to measure the distortion of the reactor $\bar{\nu}_e$ energy spectrum as well as the decrease in its overall flux, almost identical background environments for near and far detectors, and movable detectors to allow a direct check of the relative acceptance detector modules. We believe the redundancies and cross checks included in the Braidwood design are critical to establishing an oscillation signal, and in making a well supported precision measurement.

The main features of the Braidwood experiment are summarized in Table 2. The Braidwood Nuclear Power Station has two reactor cores, each producing 3.586 GW of thermal power. The baseline experiment design has four 65 fiducial ton detectors, two at 200 m, where the oscillation probability is very small, and two at 1500 m (horizontal distance) from the reactor site, near the oscillation maximum. Both near and far detectors are located at a depth of 450 meters water equivalent (mwe), in caverns excavated from low-radioactivity dolomite limestone with a uniform and well-understood overburden.

Each spherical detector consists of a 65 ton central region of gadolinium (Gd) loaded liquid scintillator (0.2% Gd by weight) contained in a clear acrylic sphere 5.2 m in diameter, which is then surrounded by an outer mineral oil volume contained in a steel sphere 7.0 m in diameter, as

Table 1: Baseline Braidwood reactor and experiment quantities.

Parameter	Value	
Number of reactor cores	2	
Thermal power per core	3.586	GW
Error on reactor power	2	%
Reactor capacity factor	92	%
Detector fiducial volume	65	tons
Detector depth	450	mwe
Detector efficiency	75	%
Number of near (far) detectors	2 (2)	
Near detector baseline	270	m
Far detector baseline	1510	m
^{9}Li/^{8}He rate after veto	0.018	$t^{-1}d^{-1}$
^{9}Li/^{8}He rate uncertainty	20	%
Other backgrounds rate after veto	0.015	$t^{-1}d^{-1}$
Other backgrounds rate uncertainty	30	%

Table 2: Estimation of the statistical and systematic uncertainties.

Source of Uncertainty	%
Relative Normalization for each Near/Far Detector Pair	0.3
Far Detector Statistics	0.2
Near Detector Statistics	0.04
Backgrounds	0.15

described in Section 2.2. Approximately 1000 8-inch photomultiplier tubes (PMTs) are mounted in the mineral oil to the surface of the steel sphere. Each detector is surrounded by systems of passive and active shielding to identify and suppress backgrounds as described in Section 2.3. The use of large fiducial volume detectors is both economical and provides important handles on systematic uncertainties, such as the radial dependence of radioactive backgrounds and external neutrons, with a large part of the fiducial volume located far from any containment walls.

Reactor $\overline{\nu}_e$s are detected via inverse β-decay: $\bar{\nu}_e$ + p $\rightarrow e^+$ + n. The experimental signature is the coincidence between the prompt e^+ signal and the delayed, $\sim$ 8 MeV signal from photons resulting from n capture on Gd. To measure the oscillation probability, the Braidwood Experiment will compare the $\bar{\nu}_e$ interaction rate in the fiducial mass at the far site to the identical mass located at the near site. This technique results in cancellation of many common systematic uncertainties, including uncertainty in the reactor $\bar{\nu}_e$ flux and the inverse β-decay cross section, permitting a precise relative measurement.

The significant uncertainties that limit the sensitivity of the Braidwood Experiment (see Table 1) are the uncertainty in the background rate, the relative normalization of the near and far detectors, and statistics. Backgrounds will be studied in detail and rates measured as described in Section 2.3. Contributions to the relative normalization uncertainty are summarized in Table 3. These uncertainties rely on careful detector construction to ensure nearly identical detector acceptance, and extensive *in situ* calibration (see Section 2.4). For detector construction, it is particularly important that near and far detectors be simultaneaously filled with the same scintillator. Table 3 also shows the precision of two cross checks, described in Section 2.5, which allow us to verify the indicated combinations of quantities affecting the measurement. Finally, statistics are increased relative to previous experiments such as CHOOZ [8] and Palo Verde [9] by using larger detectors

Table 3: Systematic Uncertainties on Relative Acceptance between Each Near / Far Detector Pair

Quantity	Uncertainty (%)	Comment	Cross checks	
			Near site cross calibration*	^{12}B production
Solid angle (baseline)	0.1	From survey: $\Delta L_{near} = \pm 10cm$		
Detector mass	0.2	volume measurement	$\surd$	$\surd$
Neutron capture E cut	0.1	E scale from n-Gd capture peak	$\surd$	
Positron E cut	<0.1	E scale from n capture peaks, ^{12}B	$\surd$	$\surd$
Optical model	0.2	Optical, source calibration	$\surd$	
Timing cuts	<0.1		$\surd$	
Total	0.3		$\sigma_{check} \sim 0.3\%$	$\sigma_{check} \sim 0.5\%$

* Note that the near site cross calibration measures the combination of the checked effects at the time of the cross calibration. Some uncertainties, such as energy scale, will have additional time dependent effects.

and a longer run.

The projected sensitivity of the baseline experiment for $\Delta m^2 = 2.5 \times 10^{-3}$ eV^2, using the assumptions listed in Table 2 and the parameters and uncertainties given in Table 1, is shown in Fig. 3 as a function of Braidwood running time for rate only, shape only, and a "rate plus shape" combination. The rate and shape measurements separately add redundancy in the signal extraction method that we regard as being absolutely essential to establish a believable observation, followed by a precision measurement of the mixing angle. As a function of Δm^2, the sensitivity of the Braidwood experiment for three years of data is shown in Fig. 4 for 90% CL for a rate versus shape measurement and in Fig. 5 for a combined rate plus shape measurement at 90% Cl as well as at the 3 and 5 σ level. The figures clearly show that the Braidwood experiment has discovery potential and the ability to establish a signal for $\sin^2 2\theta_{13} > 0.01$ and can limit the value down to values as low as 0.005 for the currently allowed Δm^2 range shown by the horizontal lines at 1.5×10^{-3} to 3.0×10^{-3} eV^2. The measurement capability of the Braidwood experiment is displayed in Fig. 6 for $\sin^2 2\theta_{13} = 0.02$ and $\Delta m^2 = 2.5 \times 10^{-3}$ eV^2. The upper plot shows the one and two σ contours for a two parameter unconstrained fit to $\sin^2 2\theta_{13}$ and Δm^2 and the lower plot shows the contours constraining Δm^2 with an uncertainty expected from the Minos experiment after two years of data, $\delta(\Delta m^2) = 0.13 \times 10^{-3}$ eV^2. From these figures, it is clear that Braidwood can measure $\sin^2 2\theta_{13}$ for values above 0.01.

Since the baseline design has multiple, movable detectors, we can optimize the configuration of detectors to enhance the mixing angle sensitivity or to make cross checks of systematics. For example if a postive signal is seen, the pairs of detectors give cross checks at each site and the ability to move far detectors to the near site allows them to be cross correlated. On the other hand, if the value of $\sin^2 2\theta_{13}$ is found to be small with the initial configuration, the experiment can be reconfigured to a "phase II" design, in which the two near detectors are moved to the far site to double the fiducal mass at the oscillation maximum for further data-taking. For these reasons, we believe that the Braidwood design is unique in flexibility for the physics and in the robust control of uncertainties to reach the required sensitivity.

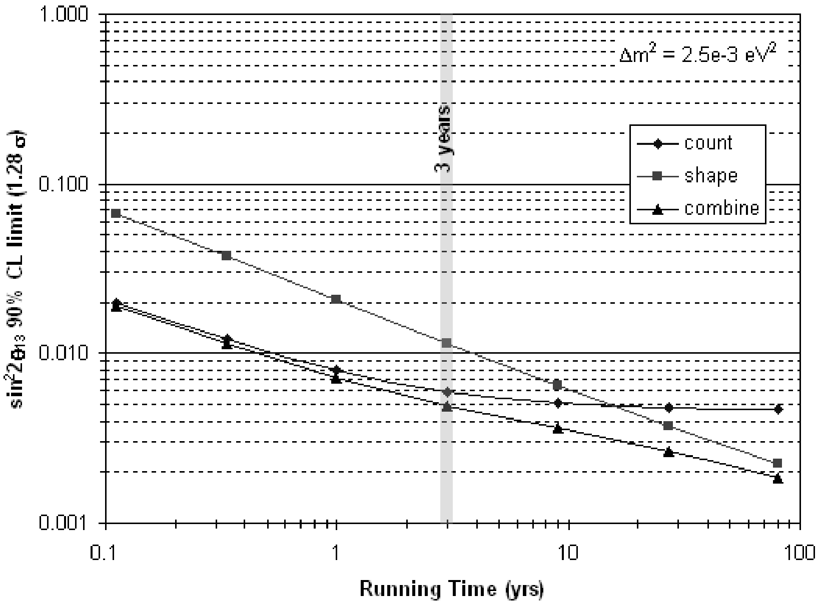

Figure 3: The 90% CL sensitivity of the Braidwood experiment versus running time for $\Delta m^2 = 2.5 \times 10^{-3}$ eV^2. The nominal data taking period is expected to be three years. The different types of fits are indicated by the markers on the line. (The Braidwood setup includes two near and two far detectors, each with 65 tons of fiducial mass, positioned at 270 m and 1510 m from two 3.59 GW reactors. With this setup, three years of running corresponds to a luminosity exposure of 2,800 GW-ton-years in the far detectors.)

2.2 Two-Zones vs. Three-Zones

In this proposal, we have adopted a baseline detector design with two zones: an inner active Gd-loaded scintillator volume and an outer mineral oil volume. There has been extensive discussion in the literature of a three-zone design, in which there is an intermediate unloaded scintillation volume between the Gd-loaded region and the mineral oil buffer. The arguments for the three-zone design are that it simplifies the response to neutrons, by catching capture γ rays which 'leak' out of the Gd-loaded volume; that it ensures that all positrons associated with neutron capture events on Gd will have an energy above the annihilation edge; and that it provides a means of tagging fast neutrons which enter the inner volume and produce an apparent correlated pair. In smaller detectors, the 3-zone design mitigates edge effects that are not a significant issue for a mid-size detector such as those proposed for Braidwood. In a multiple (near and far) detector experiment, these issues can all be overcome with a two-zone design, and the advantages of the two-zone design outweigh those of a three-zone design. Part of our work under this proposal will be to explore the efficacy of the two-zone design fully, and to quantify the cost implications of both two- and three-zone designs.

A two-zone detector has the great advantage of simplicity of design and construction, and the resulting shorter design time and reduced cost. We also believe that the two-zone detector will be far easier to calibrate than a three-zone detector. Knowledge of the relative responses of the near

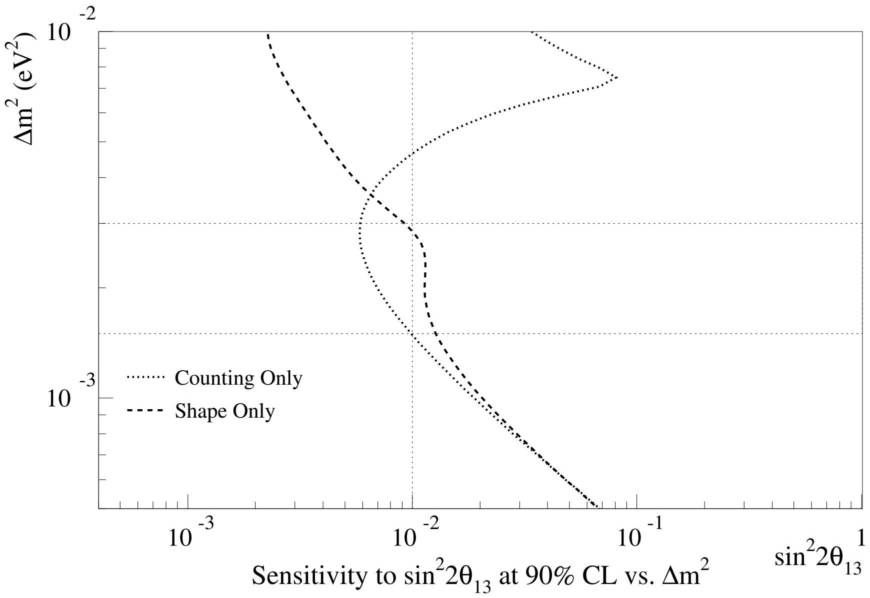

Figure 4: The 90% CL sensitivity to $\sin^2 2\theta_{13}$ as a function of Δm^2 for the Braidwood baseline experiment (3 years and 130 tons of far fiducial mass). The two curves display fits using rate-only or shape-only information as described in the text. The horizontal lines indicate the current 2σ limit on Δm^2 and vertical line marks the sensitivity goal of $\sin^2 2\theta_{13} = 0.01$.

and far detectors is critically important to the 1% disappearance measurement we are trying to make, and therefore the ability to calibrate the detectors carefully and credibly is a prime concern.

The optical calibration of the near and far detectors will provide a means for the reconstruction of event energy, as well as inputs to the detector models which will be used to help determine the systematic uncertainties on the relative detector responses. In a two-zone detector, measurement of the extinction and scattering lengths of all three optical media (inner Gd-loaded scintillation volume, containment vessel, and mineral oil) can be done by deploying normalized optical and radioactive sources inside the inner volume and in the mineral oil volume. For a three-zone configuration, however, the only way to measure the properties of all five media is to deploy sources within the intermediate volume as well. Without such a deployment, untangling the effects of the extinction and scattering by the containment vessels from those of the unloaded scintillator would be very difficult, if not impossible. Deploying normalized sources (preferably the *same* source) in all three regions is a difficult task which would require additional design time and cost.

Our preference for a two-zone design is based on the need to understand relative efficiencies between near and far detectors rather than absolute detector efficiencies. Most of the relative efficiency – the dependence of the detector acceptance on knowledge of the energy scale and resolution – can be determined *in situ* with the neutron capture events themselves. As shown in Fig. 7, the Gd capture peak is narrow enough that it can be used to provide an excellent measure of the relative energy scale of different detectors. Most importantly, unlike any potential calibration source, the neutrons integrate over the detector volume and livetime in exactly the correct way. Based on our MC simulations, we find that adjusting the energy scale to match the neutron peaks

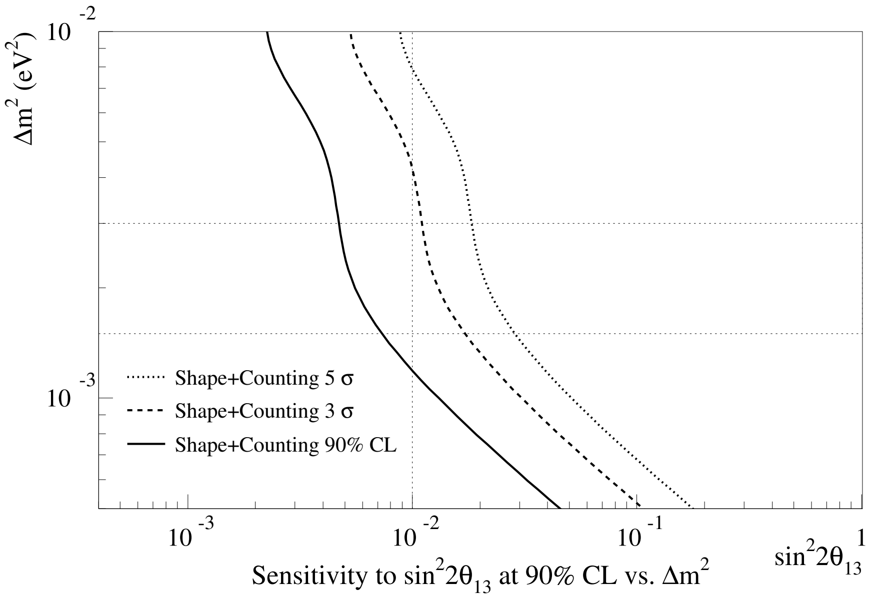

Figure 5: The 90% CL, 3σ, and 5σ sensitivity to $\sin^2 2\theta_{13}$ as a function of Δm^2 for the Braidwood baseline experiment (3 years and 130 tons of far fiducial mass). The fit use a combination of rate and shape information as described in the text. The horizontal lines indicate the current 2σ limit on Δm^2 and vertical line marks the sensitivity goal of $\sin^2 2\theta_{13} = 0.01$.

in the near and far detectors virtually eliminates acceptance differences arising even from huge (10%) differences in the energy scale between the two detectors. Figure 8 shows the comparison of the relative acceptance as a function of a shift in the energy scale before and after matching the neutron peaks, for various positron energy thresholds.

Our simulations also show that the total positron leakage below the annihilation edge in a two-zone detector is a few percent or less (and of course gets smaller with a larger fiducial volume), and depends almost entirely on geometry. We expect therefore to know this already small fraction very well, and the neutron peak calibration will help to reduce any other uncertainties associated with knowledge of the energy scale near threshold.

A two-zone detector also maximizes the size of the fiducial volume for a given detector radius. In addition to increasing the statistics of the antineutrino signal, the extra volume can be used to help identify backgrounds from fast neutrons. Neutrons entering the detector may create recoil protons near the edge of the volume, followed by a second physically separate recoil as they travel farther inward, and finally γ's from their capture on Gd. This topology – two scattering vertices in the prompt signal (with one near the fiducial edge) followed by a neutron capture signal – acts as a tag for some fraction of the fast neutron events. The tagged events will help help us to measure the background from fast neutrons in our signal sample. The additional active Gd-loaded volume in a two-zone detector thus provides similar information to the unloaded volume in a three-zone detector.

With fewer optical media, a two-zone design will also allow more photons to reach the PMTs than a three-zone design. The gain in photon statistics improves the energy resolution, thus sharp-

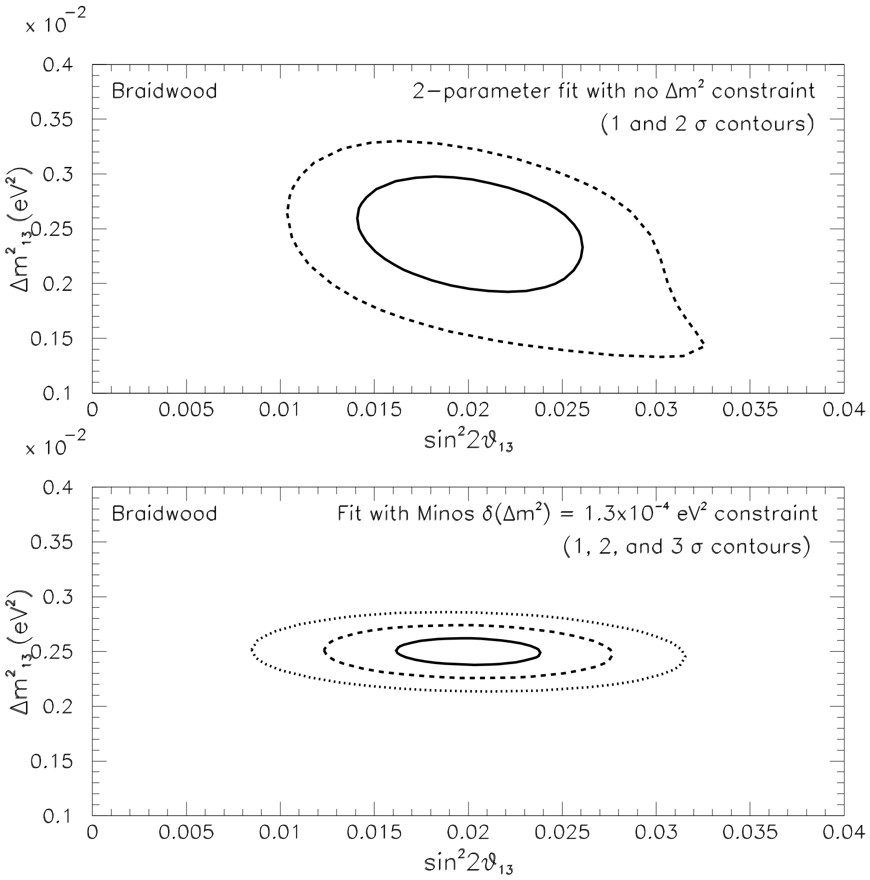

Figure 6: Combined rate plus shape fit results for observed data from three years of Braidwood data with an oscillation signal corresponding to $\sin^2 2\theta_{13} = 0.02$ and $\Delta m^2 = 2.5 \times 10^{-3}$ eV^2. The top figure gives the one and two σ contours with no external constraints on Δm^2. The bottom figure shows the one, two, and three σ contours with Δm^2 constrained with an uncertainty of 0.13×10^{-3} eV^2 corresponding to the Minos expectation with two years of data.

ening the positron annihilation edge and providing better separation between the signal and the low energy backgrounds. Fewer media also means there are fewer opportunities for a difference to arise between the near and far detectors.

2.3 Backgrounds

This section addresses backgrounds related to the θ_{13} measurement; the background discussion for the $\sin^2 \theta_W$ measurement is given in Section 4.

2.3.1 Overview

The ~ 30 μs coincidence between e^+ annihilation and n capture on Gd provided by the $\bar{\nu}_e p \to e^+ n$ signal reduces all serious background sources to a neutron capture on Gd in association with a correlated or uncorrelated in-time energy deposition from another neutron or a radioactive decay

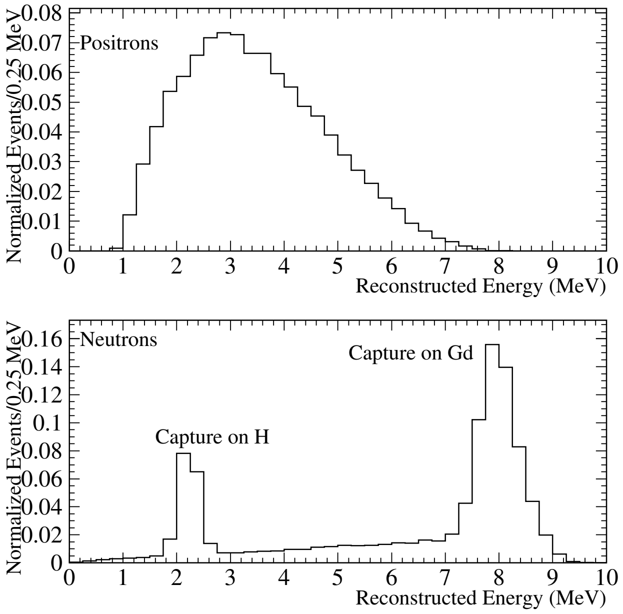

Figure 7: Simulated reconstructed energy spectra for positrons (top) and neutrons (bottom).

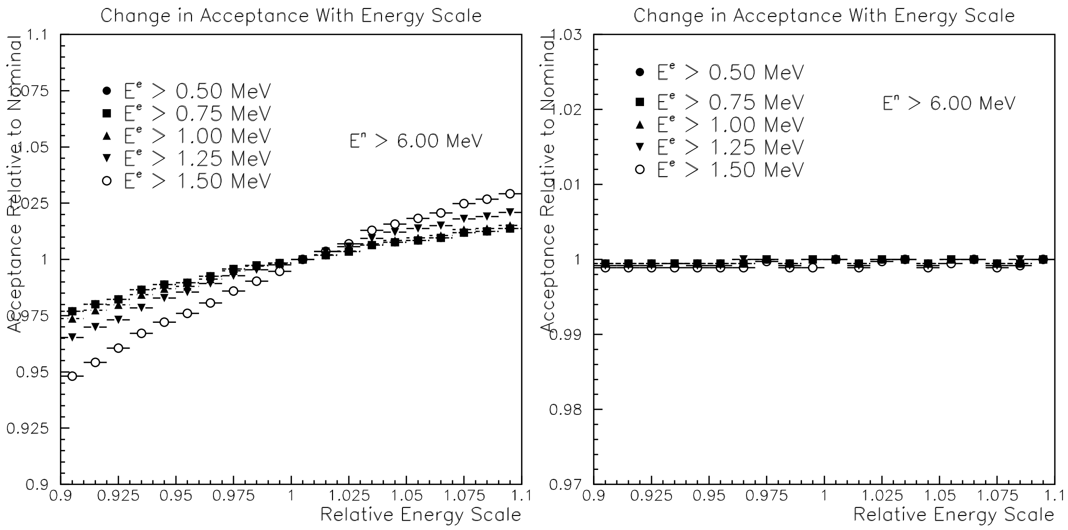

Figure 8: Acceptance as a function of energy scale shift: left panel – without a correction based on the Gd neutron capture peak; right panel – with a correction based on Gd capture peak.

in the detector. The correlated background has long been recognized as the most important. It arises almost entirely from cosmic ray muon spallation that creates the radionuclides ^{9}Li and ^{8}He inside the detector, and from spallation events in the experimental enclosure walls or shielding system that produce fast neutrons which then enter the detector. ^{9}Li/^{8}He each produce a neutron in their beta decays that mimics the antineutrino signature closely. Their 100-200 ms half-lives mean that it is difficult to veto these events by using a simple muon track coincidence without introducing prohibitive dead time. Braidwood should reduce this limitation significantly with a sophisticated veto system that provides both muon track location in the detector and a measure of the total energy associated with muon interactions in the surrounding rock. As discussed below, this information can be used to remove ^{9}Li/^{8}He events offline. Fast spallation neutrons can enter the signal sample through a sequence of hard elastic scatters with protons in the detector that produce 1-8 MeV of visible energy, mimicking a positron signal, that is then followed by the capture of the neutron through thermalization. Spallation neutrons also dominate the uncorrelated backgrounds, which occur when a neutron capture by chance takes place in coincidence with an energy deposition in the detector initiated by radioactive decay or by an independent spallation event. Braidwood will suppress fast spallation neutron backgrounds with its innovative active veto coupled with almost 2 mwe of passive shielding between the outer active veto and the fiducial detector volume.

These neutron-driven background rates may be theoretically uncertain to 50% for fast spallation neutron production, and perhaps a factor of 3 for radionuclide production. This places high demands on the signal-to-background ratio in each Braidwood detector in order to achieve an overall 1% sensitivity on $\sin^2 2\theta_{13}$, and, at the same time, calls for a designed-in capability to measure backgrounds in place. Despite these challenges, extrapolations from previous experiments and other studies indicate that these requirements can be met, provided that the detectors are at sufficient depth, that an effective active and passive shielding scheme is implemented, that radioactive impurity levels are kept under control, and that a robust triggering and data acquisition system is implemented.

The remainder of this section provides more details on background rate calculations; suppression strategies for fast neutrons, cosmogenic radionuclide sources, and intrinsic radioactivity; and *in situ* background measurement techniques.

2.3.2 Muon Flux and Neutron Production

All estimations of cosmogenic backgrounds require an accurate characterization of the muon flux at the detector. This mandates development of a good Monte Carlo generator tuned to external data and to the local geology as determined from bore hole samples (which are currently being obtained at the Braidwood site). Preliminary calculations[11] that employ a muon flux at the surface tuned to data and using GEANT4 to propagate the muons through a flat "standard rock" ($A = 22$, $Z = 11$, $\rho = 2.65$ g/cm^3) overburden appropriate for Braidwood yield flux and rate values for muons given in Table 4. The values are consistent at the 15% level with computations with the MUSIC[12] package that employ the Gaisser parameterization[13], and with determinations by CHOOZ[14] for similar depths.

Muons with energies between 50-200 GeV, the energy range where the muon flux peaks, produce neutrons through several processes of comparable importance, including direct muon-spallation, nuclear photodisintegration, and spallation by secondary pions and neutrons from muon-nucleus induced hadronic showers. Inclusive production rates are estimated by convoluting cosmic ray muon spectra with neutron muon-production formulae provided by Wang et al[15].

Of particular interest are the long-lived $\mu + {}^{12}C, {}^{13}C$ spallation products ^{9}Li$\big(Q = 13.6$ MeV, $\tau_{1/2} = 178$ ms$\big)$ and ^{8}He$\big(Q = 10.7$ MeV, $\tau_{1/2} = 119$ ms$\big)$, with 49.5% and 16.1% branching fraction $\beta + n$ decay modes, respectively. The correlated electron ionization/neutron capture signature from these radionuclides can easily mimic the $\bar{\nu}_e p \rightarrow e^+ n$ signal. Furthermore, the decays occur so long after

Table 4: Muon and cosmogenic neutron properties expected at the baseline Braidwood depth of 450 mwe. Muon rates and energies are from Ref. 11. Inclusive neutron rates are obtained by convoluting these muon rates with production spectra from Ref. 15. The upper numbers for radionuclide rates are obtained by assuming the same exclusive/inclusive production ratios at KAMLAND as obtained from Ref. 16. The lower rates are from Horton-Smith's model described in Ref. 17.

Quantity	**D=450 mwe**
$\bar{\nu}_e$ interaction rate– near detector	55 day^{-1}ton^{-1}
$\bar{\nu}_e$ interaction rate– far detector	1.8 day^{-1}ton^{-1}
mean muon energy	107 GeV
muon flux	0.21 m^{-2}s^{-1}
7 m detector muon rate	8.1 Hz
inclusive neutron production rate	167 day^{-1}ton^{-1}
7 m detector unvetoed neutron rate	1.5 n / detector / day
^{12}B/^{12}N production per day	3.7 day^{-1}ton^{-1}
^{8}He/^{9}Li production per day	0.016-0.07 day^{-1}ton^{-1}

the passage of the initiating muon track that simple veto schemes are ineffective in removing them from the signal sample. Production estimates for ^{9}Li/^{8}He are obtained by assuming that the ratio of radionuclide to inclusive spallation neutron is the same as in KAMLAND[16]. The radionuclides ^{12}B $\left(Q = 13.4 \text{ MeV}, \tau_{1/2} = 20.2 \text{ ms}\right)$ and ^{12}N $\left(Q = 17.3 \text{ MeV}, \tau_{1/2} = 178 \text{ ms}\right)$ production rates are given as well since they provide spallation rate monitors and serve as useful calibration sources; their rates are estimated by the same procedure. Horton-Smith has argued[17] that this technique overestimates radionuclide production rates at shallow sites (in particular, CHOOZ) by a factor of $4-5$ because the bulk of the production at KAMLAND is due to hard secondary neutrons that produce spallation nuclei in the detector; and the production rate for these energetic secondaries decreases more rapidly with energy than the inclusive neutron rate in scaling to the softer cosmic ray spectra of Braidwood or CHOOZ.

2.3.3 Fast Neutron Shielding

Fast neutron background will be reduced through the use of a system of passive absorber and active detectors which completely surround the steel vessel. As a first step, two approaches have been studied: 1 meter of heavy concrete with detectors mounted on the outside (and possibly on the inside) and 2 meter thick water or scintillator viewed by photo-tubes.

We have assessed the performance using two different calculations of the fast neutron correlated background. Both studies use the muon spectrum at 450 MWE from Pilcher & Hurwitz[18]. In the first study, the fast neutron spectrum is computed using the calculation of [19] and gives a production rate of 177 n/ton/day in the rock surrounding the detector. The neutrons are then transported toward the detector using the MARS code and we find 4,200 n/day emerge from the rock. Taking into account propagation through the shield and 50 cm of mineral oil buffer and an 88% chance of triggering the veto, a total of 0.7 background events per day are expected.

A second calculation uses GEANT4 [21] to handle all the particle interactions. The simulation includes interaction with the detectors in a realistic way. The predicted neutron production rate of of 167 n/ton/day agrees well with the previous calculation, as does the rate of 4,500 n/day emerging from the rock. The calculation gives a total rate of 0.2 background events per day. Aside from the input muon spectrum, the two calculations are independent. The next step is to use the full GEANT4 simulation to determine how well the neutron and spallation isotope backgrounds may be measured.

Several designs for the veto and shield system have emerged. For passive shielding, 1 m heavy concrete (with a density of 3.5) could be used with resistive plate chambers or large proportional tubes. For active shielding, 2 m of water of scintillator viewed by photo-tubes appears to be adequate. All of our designs allow the neutrino detectors to be moved for cross calibration. From a cost point of view, there are no show stoppers, although the costs between the designs.

2.3.4 Suppressing Cosmogenic Radionuclides

Backgrounds from spallation-produced radionuclides produced inside the detector are harder to eliminate due to the long half-lives of ^{9}Li and ^{8}He and the nearly identical detector response of these correlated $\beta - n$ decay pairs to the e^+n antineutrino production signal. Fortunately, measurements at CHOOZ[14] and KAMLAND[16] indicate that ^{9}Li/^{8}He cross sections are tolerably small ($S/B \gtrsim 10$ with no cuts); and there are some prospects for improving the precision of these measurements on the short term at KAMLAND. It would be valuable, however, to obtain further constraints on these and other radionuclide production rates at depths more similar to Braidwood's at something like the VSPLAT facility [10].

Extra handles[16] available using the data itself include: (1) an ability to remove events off-line in which the positron-like primary ionization signal is spatially correlated with the track position of a muon passing through the detector within a specified time window before the event of interest, (2) an ability to remove events offline in which the neutron capture is correlated with a muon-induced shower independently measured in the detector and the veto system, and (3) the possibility of constraining the ^{9}Li/^{8}He production by examining positron like energies between 9 and 14 MeV, which correspond, respectively, to the maximum of the $\bar{\nu}_e$ reactor flux and the maximum β-electron energy in the radionuclide decay. Implementing the first procedure requires study of the muon tracking resolution, the neutrino detector vertex resolution, the optimal time window, and the data acquisition scheme. Implementing the second requires similar studies plus development of a procedure to identify a muon-induced shower using the veto system, either alone or with the neutrino detector.

In principle, it is possible to discriminate via pulse shape analysis neutron-generated proton recoils from the ionization/annihilation signal from $\bar{\nu}_e$-induced positrons, although this technique has enjoyed limited use to date. Implementing this scheme in Braidwood would require an R&D program in fast neutron and recoil proton response in the scintillator and oil, and a method to monitor and calibrate the technique during actual data taking.

2.3.5 Controlling Intrinsic Radioactivity

Beta and gammas from U, Th, and K decay chain products in the PMT glass, scintillator, support structures, and atmosphere can produce ≥ 1 MeV energy depositions in the detector that can form an accidental coincidence with a stray neutron produced by neutron spallation in the external rocks.

Procedures must be developed to limit U/Th levels to $\sim 10^{-12}$ g/g concentrations in the scintillator and $\sim 10^{-10}$ g/g in the acrylic; the tolerances for K are two orders of magnitude less stringent. These levels are well above those achieved by KAMLAND, BOREXINO, and SNO (although these experiments do not use Gd-doped scintillator); and they have been achieved in the past by the Palo Verde and CHOOZ experiments. It is worth noting that potential risks of dangerous indirect U/Th backgrounds induced by Rn production in the rock caverns are considerably reduced by the low activity dolomite limestone geology that predominates at Braidwood.

A procedure must be developed to insure that the Gd does not carry contaminants into the system; this will require chemical methods for purifying the scintillator and Gd separately before making the final mixture, as was done in Palo Verde and CHOOZ. Assuming these levels can be achieved in the scintillator and acrylic, then the singles rate is expected to be dominated by PMT radioactivity, where K(U/Th) levels of 60 ppm(30 ppb) can be achieved using low radioactivity glass. The critical detector parameter for determining the singles rate from radioactivity is the thickness of the outer mineral oil buffer. This must be studied carefully using Monte Carlo techniques both to optimize the overall experimental S/B (a thinner buffer means more signal and more background), and to account for the complicated PMT geometry at the outer wall, the mineral oil-acrylic wall interface, and other non-trivial material and geometric effects.

2.3.6 *In Situ* Monitors

Background rates *must* be measured; and it is therefore imperative to design the triggering and data acquisition system to tag and record as many of the important types of these interactions as possible. As an example, ^{12}B and ^{12}N will be relatively copiuosly produced by muon spallation of carbon. Their high Q β-decays occur without an unaccompanied neutron at time scales comparable to the more dangerous ^{9}Li/^{8}He. Thus, they provide a clean monitor reaction for spallation-induced radionuclide production (as well as a useful calibration source in the detector). For both types of spallation backgrounds this can be accomplished by ensuring that the data acquisition system is capable of tagging muon tracks in coincidence with a delayed neutron signature. Issues to decide include the aforementioned required tracking resolution of the veto system and the specific triggering schemes. Extending the area of the active veto beyond the size of the enclosure roof would permit better studies of fast neutron production in the surrounding rock.

Uncorrelated background rates can be measured in the data by examining neutrino candidate events in which the neutron-like energy signal comes in at many capture time constants after the positron-like signal, or by selecting events using the "swap" technique[22], wherein the positron selection criteria are interchanged with the neutron selection criteria. An ability to tag the 164(0.3) μs time correlated ^{214}Bi-^{214}Po(^{212}Bi-^{212}Po) $\beta\alpha$ decays from the ^{238}U(^{232}Th) chain will allow constraints to be placed on contributions from radioactivity in the oil and acrylic.

Finally, one should acknowledge that the very best background monitor of all arises from reactor-off running. The Braidwood Power Station's operating efficiency is so high that it is highly unlikely that both cores will be non-operational for any significant period of time. On the other hand, neutrino flux will drop by a factor of two for about one month intervals that occur every nine months to permit refuelling. Reactor power information should be available throughout the run, so that occasional power reductions at the complex can be exploited in offline analyses.

2.4 Calibration

For a multi-detector reactor experiment, we need only understand the ratio of acceptances between the near and far detectors, and not the absolute detection efficiency of individual detectors. The detection efficiency ultimately depends on what cuts we choose in our final analysis, but we will assume here only cuts on the positron and neutron energies, and the coincidence time between the positron and neutron signals. The difference in overall detection efficiency between the two detectors then depends primarily on a small number of response parameters for each detector:

1. The number of hydrogen targets
2. The Gd loading fraction
3. Scintillator light output, including aging effects
4. Detector optics, including the attenuation lengths of the different media (five for a three-zone detector, three for two-zone), PMT angular and wavelength response, Rayleigh scattering, and diffuse and specular reflection off all media
5. Number of working PMT's, as well as their individual gains and efficiencies
6. Number of working electronics channels and individual efficiencies
7. The livetime

All of these items may change with time, and furthermore can create position dependences within the detector which in turn may depend on time. The parameters can be measured individually and then used in the context of a detector model (such as a Monte Carlo simulation) to predict the relative detector efficiencies, or they can be measured in an integral way by using a source identical or nearly so to the antineutrino signal. In practice, we expect that we will use both approaches, and in so doing not only be able to calibrate the two detector efficiencies relative to one another but determine the systematic uncertainty on the calibration.

The primary goals of the calibration program are therefore:

- To measure differences in the two integral detector responses directly through radioactive source deployments, *in situ* calibrations (spallation products and neutrons from reactor antineutrinos), and possibly detector movement
- To measure the individual response parameters in order to build detector models for use in the efficiency calibration and the determination of the relative systematic uncertainties between the detectors
- To provide an analytic form of the detector response so that each event's measured PMT hits, charges, and times can be re-mapped into event energy [2]

For the first goal, we will need to be able to deploy various radioactive sources at many positions within the volumes of both detectors (using the same physical source for each detector). We will investigate adding a short-lived dissolved source to the scintillator (uniformly mixed) to mimic the spatial distribution of anti-neutrino induced events. We also need to be able to accurately

[2] We note that with a multi-detector experiment, such an explicit reconstruction of event energy is not strictly necessary. The differential response function for the near and far detectors can be cast to map neutrino energy into observed hits and charges, rather than into observed energy, removing the energy calibration step.

tag cosmic-ray spallation products, so that they can be used as calibrations and checks which can illuminate the entire active detector volume.

Fior the second and third goals, we will need to deploy optical sources of various wavelengths both inside and outside the active volume, at as many points as are necessary to measure the bulk optical properties of all the detector media. We will also need to develop a full detector model which includes the light generation (both scintillation and Cerenkov light), propagation (using the measured optical parameters), and detection.

Well before the design of the detectors and calibration systems, several basic questions need to be answered: At how many positions within the detector volume will sources need to be deployed? How well do the angular and wavelength distributions of optical sources need to be known – and how well can they be known in a low-cost, practical system? How well must the source position be known to calibrate the position-dependence of the response functions? Can there be differences between the detectors which are not seen by *in situ* calibrations like the inverse β-decay neutron capture peaks, and cosmic-ray spallation nuclei? How well matched do radioactive sources need to be to the expected signal and backgrounds, in order to be useful?

Much of the work to answer these questions will necessarily be done by simulation. For such a simulation to be useful, it must be based upon input parameters taken from measurements of the actual detector media. Many of the planned measurements are discussed in Section 2.6.

2.5 Cross Checks

In-situ calibration systems — such as radioactive sources, and laser or LED light sources — will play a large role in understanding the efficiency and energy scale, but the hydrogen density and target volume cannot be determined in this way. The Double-CHOOZ collaboration [6] has proposed using various control and measurement procedures during detector assembly to ensure that the target vessels and target chemistry are identical, but even in their best case scenario they are only able to get the uncertainty on the relative normalization down to 0.6%. While we intend to implement similar procedures during assembly, the Double-CHOOZ plan does not provide a way to verify that the assumed precision of these methods is correct. The plan for Braidwood is to construct multiple, movable detectors which will allow an independent, high precision measurement of the relative detector normalization.

2.5.1 Moving Detectors

The reactor neutrino flux itself provides one of the best means of determining the relative normalization of near and far detectors. One can use the near detector site, where the interaction rate, or flux, is 30 times larger than at the far site, to compare pairs of detectors. By placing two detectors side-by-side in the near detector hall, where both detectors experience the same flux, one can determine their relative normalization ($\equiv \frac{N_1}{N_2}$), at that moment in time, with the statistical precision determined by the number of events observed. Given the Braidwood neutrino flux, the baseline detector size and near site location, a statistical uncertainty of 0.3% could be achieved in fewer than 100 days of side-by-side calibration running (less than 10% of the proposed experimental run).

This direct measurement of the relative normalization determines the relative target volume and hydrogen content for the two detectors. This relative normalization can be applied when one of the detectors is moved back to the far location since the hydrogen content and target volume are constant if the temperature is kept constant. If the detector efficiency can be shown to be stable, for example by comparing the multiple detectors at each site, then the uncertainty in relative normalization will reach the lower limit set by the side-by-side calibration. This hypothesis could also be firmly established by comparing side-by-side calibration runs taken early in the experiment to those taken at the end.

2.5.2 Multiple Detectors

The requirement of movable detectors puts limits on the detector size and weight. These limits are set by shaft and tunnel apertures, and by the capacity of the crane or other lifting system. Multiple detectors allow one to achieve the desired target mass within the constraints set by a practical and cost-effective facility design. In the Braidwood experimental baseline, two far and two near detectors are assumed. The use of multiple detectors at both the near and far site will allow the systematic uncertainties between multiple detectors to be studied directly with cross checks. In addition, the extra target mass at the near site gives the Braidwood experiment the potential to measure the weak mixing angle.

Multiple far detectors may also improve the experiment sensitivity if the relative normalization uncertainties between the n far detectors are uncorrelated. Combining measurements from the multiple detectors could reduce the overall effective relative normalization by up to a factor of $1/\sqrt{n}$. The requirement of uncorrelated uncertainties is satisfied if the uncertainties come from independent measurements such as separate side-by-side calibration runs.

Multiple movable detectors allow for greater flexibility in operating the experiment. For example, if it turns out that $\sin^2 2\theta_{13}$ is very small, then it is possible to redeploy one or both of the near detectors at the far site (or to build additional far detectors) to increase sensitivity to the spectral shape distortion [3].

2.5.3 ^{12}B Production

A unique feature of the Braidwood site is a uniform and well-understood overburden with the ability to place near and far detectors at nearly identical depths. Therefore, muon and associated spallation rates should be essentially the same for all detectors. This would afford us the ability to perform an accurate, relative calibration of fiducial volumes based on the observed rates of ^{12}B production in each detector. This isotope is largely produced via (n,p) reactions from secondary neutrons following muon interactions in carbon-rich materials (such as scintillator), though muon capture also contributes. ^{12}B undergoes β-decay with an endpoint energy of 13.4 MeV and has a half-life of 20.2ms, so it could be reasonably well tagged to the progenitor muon. We expect to see about 150 such events per day in each 65-ton detector for an overburden of 450mwe, based on references (Galbiata and Beacom, hep-ph/0504227) and (Hurwitz and Pilcher). Thus, the number of ^{12}C targets in each detector could be measured to a statistical accuracy of 0.43% in one year of livetime.

In order to keep systematic uncertainties below this level, several conditions are required: **1)** The detectors must be placed at similar depths. This is due to an uncertainty in the predicted, relative production rates as a function of depth, which is very diffult to define at the percent-level owing to a dearth of experimental data. However, if the difference in overburden is, say, 10mwe, the rate correction need only be known to within 20%. **2)** Based on the expected change in production rates with depth, the relative overburdens must be known to within ~2mwe. This should be achievable based on the measured muon flux at each detector. **3)** The detectors must be deeper than ~400mwe. This is to insure that the average muon rate crossing each 65-ton detector is low enough to allow for more than ~4 ^{12}B half-lives between successive muons so as to allow for reasonably efficient tagging. This will be important to reduce the background due to neutrino interactions in which the neutron signal falls outside of the acceptance window, resulting in apparently uncorrolated events which could be mistaken for ^{12}B decays. At the near site, the total number of such events could be comparable to the actual number of ^{12}B decays. However, the ability to fit the decay curve over several half-lives should reduce the impact of this to a modest level, such that the overall uncertainty in the relative rate measurement is expected to be 0.5% per detector per year of livetime. Thus, we expect to be able to cross-calibrate any two detectors to this level after two years of livetime using this technique.

2.6 Questions and proposed R&D

If the Braidwood experiment is to be done in a timely fashion, three areas will require substantial R&D support during the coming year. These areas, discussed in detail in Sections 3.1 - 3.3, are: 1) engineering studies to prepare an accurate cost estimate and schedule for civil construction at the Braidwood site; 2) mechanical engineering for the spherical detectors and their support and transport; and 3) R&D on the properties, stability, chemical compatibility and large-scale production and handling of Gd-doped liquid scintillator.

Complementary to these major projects are investigations of important questions that can be pursued by collaborating institutions largely with funds from their base grants. Most of these investigations involve simulations or obtaining data for inputs to simulations; they are ideally suited for supervised participation of undergraduates. Support of these undergraduates is an important part of the education and outreach component of this proposal.

The paragraphs below present questions to be addressed by these smaller-scale investigations.

Detector design. As discussed in Section 2.2, the baseline detector design has two zones, rather than the three zones discussed by other groups. The two-zone design has distinct advantages in simplicity of construction and deployment of calibration sources, and preliminary studies indicate that its performance will be very good in an experiment in which uncertainties in relative (rather than absolute) detector response are important. Before we commit to this baseline design, we must explore its implications carefully with more detailed simulations. So far, most of our results have come from a fast parametric Monte Carlo program; these results must be confirmed and extended with a full GEANT4 simulation, a major task. In particular, the issues of blurred positron threshold and possible compromising of the ability to tag fast neutrons must be thoroughly investigated. Significant Monte Carlo studies will also be devoted to optimization of various detector parameters, such as mineral oil buffer thickness and photocathode coverage.

Backgrounds, muon veto/tagging system and neutron shielding. As discussed in Section 2.3, the ability of the detectors to reduce uncertainties from backgrounds must be thoroughly understood through careful simulation studies of cosmic-ray spallation processes and radionuclide (^{9}Li and ^{8}He) generation. It is especially important to design the detectors and muon veto/tagging systems to measure background shapes and magnitudes *in situ*. R&D questions in this category (presented in Section 2.3) include issues of optimal coverage of active and passive shielding, tracking resolution and technology, and engineering of support structures.

Calibration. Intercalibration of detectors (discussed in Section 2.4) will use three standards: radioactive sources, optical sources, and *in situ* signals from cosmic-ray spallation products and neutrons from reactor antineutrinos. Detailed questions for investigation include: How reliable and precise are energy calibrations with radioactive sources? How precisely can the relative efficiency of neutron capture be measured with sources? How many source positions are necessary? How well must we know the positions of sources and the angle and wavelength distributions of optical sources? How will sources be deployed? Could there be differences between detectors that do not show up in *in situ* calibrations?

Scintillator properties. In addition to the substantial R&D project of developing and mass-producing a suitable Gd-doped scintillator, the characteristics and responses of the scintillator(s), and also of the non-scintillating oil, must be measured and characterized for inputs to simulations. These properties include: radioactivity levels; scattering and extinction lengths and index of refraction as a function of wavelength; Gd-capture probability and aging properties as a function of Gd loading in a narrow range of contractions ($0.1\% - 0.3\%$); median and distribution of scintillation light output (including quenching effects) for positrons, electrons, gammas, neutrons, and recoil protons; and time spectrum of generated light.

Photomultipliers. Detailed measurements of sample PMTs must be made, both to ascertain their properties in order to improve the detector simulation, and to aid in selecting a PMT vendor. Quantities to be studied include quantum efficiency; background radioactivity; dependence of PMT gain on high voltage, gain stability, and sample-to-sample variations; rates, spectrum, and dependence on temperature and on-off cycling of dark noise; "flashing" probability; failure modes; timing characteristics such as transit-time jitter and pre- and after-pulsing; wavelength-dependent angular response; and light reflection coefficients.

Based upon the experience from detectors like the Sudbury Neutrino Observatory, we believe that a large part of the point-to-point variations in response will be due to the response of the PMTs to light at different angles. For events occurring near the edge of the active volume, the near-side PMT photocathodes will on average be illuminated by high incidence angle photons. For events nearer the center, the photons tend toward normal incidence. The position sampling we will use for source calibrations will therefore depend on how steep the PMT response is with incidence angle, and this response is something we must measure now.

Electronics. Possible architectures for readout electronics must be evaluated for suitability and cost. It appears attractive to record the amplitude of signals from each PMT as a function of time, during a time window centered on a trigger. It is planned to test candidate systems with a laboratory prototype of the detector using the baseline scintillator and photomultiplier tubes. Most of this work can be done with funds already available.

Alternative PMT and Scintillator Options Members of the Braidwood Collaboration are interested in investigating alternative PMT coverage and scintillator options that could give measured signals from both Cerenkov and scintillation light, giving additional handles to suppress backgrounds. This might be done with a slow scintillation mixture with somewhat lower light production levels in order to separate the prompt Cerenkov signal with timing information. The effective photocathode coverage would have to be increased to $\sim$50% with more PMTs and light concentrators. The potential advantages of this technique are: 1) eliminating the recoil proton signals by which fast neutrons can produce correlated background, and 2) direct tagging of positrons, especially at low energies, since their annihilation would yield another $\sim$MeV of visible energy in the scintillation signal, but none in the Cerenkov component since the resulting scattered electrons from the annihilation gammas would be below threshold.

3 Proposed Engineering and R&D for Cost and Schedule Determination

In the following sections, we describe Engineering and R&D tasks for which funding is requested in this proposal.

3.1 Proposed civil engineering

3.1.1 The Braidwood Site

The Braidwood Nuclear Station is located about 90 km southwest of Chicago. The plant is built next to an old coal strip mine which has been converted into a cooling lake. The terrain at Braidwood is very flat with a change in elevation of less than two meters over the region of interest. The plant consists of two reactors, each with a rated maximum thermal energy of 3586 MW. Averaged over the last eight years, both reactors have operated with a capacity factor of greater than 90% and capacity factor has continually improved throughout this period. The two reactors are separated by about 100 meters running north-south (see Figure 9). The reactors sit in the middle of a rectangular security area. All experimental facilities must be located outside this security fence. Outside the fence, the point of closest approach is on the east side at a distance of about 200 meters from the reactors.

To achieve the required cosmic ray shielding, the detectors will be located at the bottom of shafts, one at the near site and one at the far site. (Figure 10 shows the proposed layout of the facility.) The shafts will be 115 to 170 meters (300 to 450 meters water equivalent (mwe)) deep. Geological data collected during the planning and construction of the plant [23] show a rock formation, known as the Galena/Platteville, that begins at a depth of about 85 meters and extends to nearly 200 meters. The Galena/Platteville formation is made up of dolomitic limestone, a rock type that is typically good at supporting tunnel structures. In addition, the radioactivity of limestone is typically low compared to most other rock types. The low intrinsic radioactivity of this specific rock group is confirmed by several gamma surveys performed during the original site characterization studies [23]. It is in this layer that the detector rooms will be constructed. The actual depth will be determined by the results of a core boring study that is currently in progress. The rock cores and bore holes will provide data on rock strength and water flow rates which will be used to determine the feasibility and cost of civil construction and maintenance as a function of depth. From a physics point of view, deeper shafts are preferable since background rates and dead time decrease with depth. On the other hand, depth may be a cost driver for the experiment, and it may not make sense to go below the depth at which background uncertainties cease to be a limiting systematic of the experiment. Continuing this cost-benefit analysis will be a high priority in the coming year.

3.1.2 Baseline Design

In the baseline design the detector halls are located due east of the reactors on the line that is equidistant from both reactors. The near detector hall is just outside the security fence (~200 meters) and is located 175 meters (450 mwe) below the surface. Therefore the neutrino path length distance is approximately 270 meters. The far detector hall is 1500 meters due east of the reactors and is also down 175 meters which results in a neutrino path length of about 1510 meters. The baseline calls for two detectors at each site, each with an outer diameter of 7 meters. Each detector will be surrounded on all sides by a veto system that has an array of active cosmic ray detectors outside about a meter of passive shielding. Two complete detector-veto systems will sit inside a 12 m wide × 14 m high × 32 m long cavern. Each room holds two complete detector-veto systems.

Ten meter diameter shafts connect the surface to the detector level at both the near and far sites. Each shaft contains two elevators, ventilation ducts, electrical and data cables, as well as

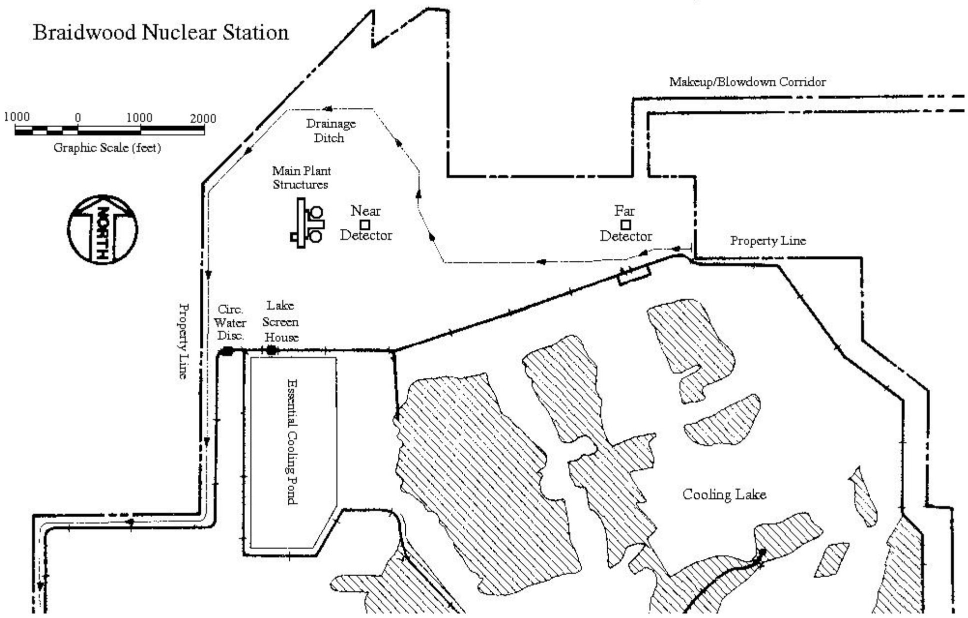

Figure 9: Drawing of the plant and surrounding area showing the approximate locations of the near and far detectors with respect to the plant and cooling lake.

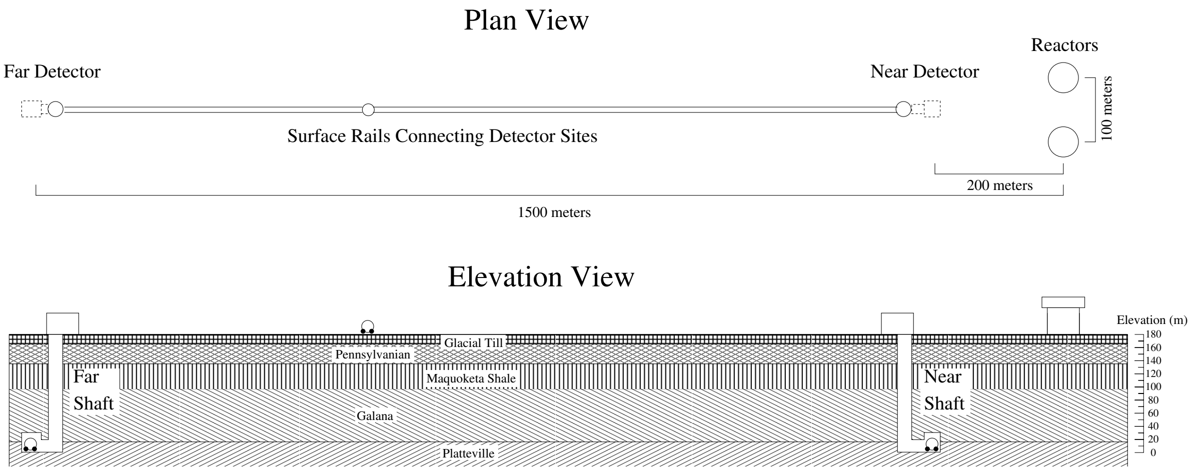

Figure 10: Plan and elevation views of the proposed layout of the experimental facility are shown. The elevation view shows the the major geological strata and their approximate elevation, in meters above sea level. Buildings, shafts and detectors are not drawn to scale.

pumps and water pipes for removing water from the shaft sump. The detector halls are connected to the shaft by a tunnel stub. At the far end this stub will be approximately 10 meters in length, which is the minimum required for structural integrity. The near tunnel stub will be about 45 meters long, because surface infrastructure at the near site does not allow construction of the shaft directly above the detector hall location.

In March of 2004, the collaboration commissioned a study of the cost and schedule of constructing an underground neutrino facility at the Braidwood site. The study was conducted by the consulting firm of Don Hilton and Associates. The results of the study were presented in such a way that cost of specific tasks could be broken out into manageable units (cost/meter of shaft, of tunnel, etc.) and rearranged to optimize the physics potential per unit cost. Table 5 show the estimated cost of the baseline civil construction as determined using the results of the Hilton study. The 17% scale factor for EDIA (Engineering, Design, Inspection and Administration) is consistent with industry standards for a project conducted under a design and build contract [24]. The 25% contingency assumes that the rock conditions along the full length of each shaft have been fully characterized, which will be the case when the shaft core borings are completed this October. The Hilton study estimates that each shaft and detector hall will take about 18 months to complete, with about 3 months on each end to mobilize and demobilize. The work on the two shafts can either be done serially or in parallel, so the civil construction should take between 2 to 3.5 years to complete.

3.1.3 Civil Engineering Needed for a Proposal Design Report

<u>Developing the Scope for a Design and Build Contract Package</u> The current plan for civil construction is to use a design and build contract [25]. In a design and build situation the collaboration specifies the layout, requirements, and baseline design, and the final design is determined by the contractor. This allows contractors the freedom to select techniques that they are already familiar with or to use equipment that they already own. The contractors know best how to use local

Table 5: The cost of civil construction for the baseline project estimated using the study of Don Hilton and Associates.

Description of Work	Quantity	Units	Unit Cost	Subtotal	Total
General Mobilization	1	each	$3,286,691	$3,286,691	$3,286,691
Shaft					
mobilization	1	each	$512,165	$512,165	
pregrout overburden	15	meters	$7,538	$113,074	
excavate & line soil	15	meters	$62,891	$943,360	
excavate & line rock	160	meters	$42,262	$6,761,941	
water ring	1	each	$87,445	$87,445	
surface facilities	1	each	$104,532	$104,532	
equipment	1	each	$664,844	$664,844	
sump room	1	each	$226,295	$226,295	
decommissioning	1	each	$412,289	$412,289	
Shaft Total	2	each	$9,825,945	$19,602,870	$19,602,870
Detector Room (each room houses 2 detectors)					
excavate	32	meters	$69,156	$2,212,981	
grout	32	meters	$5,641	$180,511	
Detector Room Total	2	each	$2,393,492	$4,786,984	$4,786,984
Tunnel					
excavation	55	meters	$28,237	$1,553,035	
grout	55	meters	$2,247	$123,585	
Tunnel Total	55	meters	$30,484	$1,676,620	$1,676,620
Subtotal					$29,353,165
EDIA	17	%			$4,990,038
Contingency	25	%			$8,585,801
Total					$42,929,004

labor, methods and means most cost-effectively. This can potentially result in a faster and less expensive overall project. The design and build process requires that the collaboration focus, early on, on developing a well-defined set of requirements that gives bidding contractors the maximum design flexibility. This will be a major activity in the next year as the collaboration prepares a full proposal.

In order to determine the requirements a significant baseline design study is needed. This study will include geotechnical, civil, electrical, and mechanical engineering. It will provide a framework for estimating cost and schedule, and for creating a bid package suitable for completing a design and build contract. The specific elements of this study, and their approximate costs, are discussed in the following paragraphs and are summarized in Table 6. The cost estimate of this study is done to a precision of $25K where each unit of $25K represents 1 senior engineer-month or 2 junior engineer-months.

Geological and geotechnical engineering tasks will include the characterization of the ground units (or strata), and the determination of the ground water table and ground permeabilities in

Table 6: Cost estimate for required civil engineering. This estimate is made in increments of \$25K where one unit of \$25K represents 1 senior engineer-month or 2 junior-engineer months.

Task	Cost (thousands of dollars)
Geology/Geo-technical	75
Civil/Structural	50
Electrical	25
Mechanical	25
Drafting	75
Cost & Schedule	25
Other Costs	50
Management & Administration	75
Detector Moving Study	25
Contingency	100
Total	525

the various units. Viable options for excavation methods, rock support systems and water control will be identified. These studies are expected to cost approximately \$75K.

Civil and structural engineers will determine the requirements for all surface work platforms and buildings. They will also determine all needed utility runs and access roads. Underground they will look at shaft lining and floor requirements. These studies have an anticipated cost of approximately \$50K.

Electrical engineering tasks include determining the specifications for power and communications: power distribution, transformers, lighting, grounding, safety systems such as fire detection, phone and internet. The estimated cost of these studies is \$25K.

The mechanical engineering studies will determine the requirements for heating, ventilation, and air conditioning (HVAC), fire protection, ground water pumping systems, and other utilities. The approximate spatial layout and routing of pipes and ducts will also be determined. The mechanical engineering cost is assumed to be \$25K.

All engineering studies will result in a reviewed outline of the determined specifications, and text for the related sections of the bid and contract documentation. In addition these engineering studies will generate the drawings required to bid the contract. These will include scale-approximate schematics of the layout of the surface buildings, shafts, tunnels, and chambers. Accurate scale drawings will be generated for the existing surface conditions; the spatial envelope of the minimum required excavations; and for the baselines of the electrical, mechanical and structural design. Drafting costs are expected to to be about \$75K.

In the course of these studies a methodology will be determined for estimating the cost and schedule. A risk analysis will be made to help in setting the appropriate contingency. These tasks have been allocated \$25K. In addition, \$50K has been allocated for "other costs." These costs include a land survey, evaluations of environmental safety and health requirements, and permitting.

Finally, \$75K is allocated to project management. These tasks will include coordinating with Exelon, the funding agencies and the institutions of the collaboration; conducting the engineering reviews; and contractor selection and pre-qualification.

Detector Moving Study The experiment baseline specifies movable detectors which allow for an important cross check of the relative normalization of the near and far detectors as discussed in Section 2.5.1. In addition movable detectors allow the detectors to be built on the surface in a single facility, during the civil construction. Without this capability, the project would incur additional costs from installing clean rooms and overhead cranes in each detector room. Also, transferring scintillator and other potentially toxic materials underground would present a significant environmental and safety hazard. Finally, detector construction, commissioning and testing could be conducted on the surface during civil construction, so that the detectors are ready to be installed as soon as the construction of the halls is completed.

The issue of how best to lift a 150 to 200 ton detector from the bottom of a 175 meter deep shaft, move it across 1300 meters of flat land, and lower it down a second 175 meter shaft must be addressed in the full proposal. The Fermilab Facilities Engineering Services Section (FESS) is currently in discussion with the Belding Walbridge Company about the cost and scope of such a study. Belding Walbridge is a contractor in heavy lifting and rigging and has worked with Fermilab in the past.

This study will occur in two phases. In the first phase Belding Walbridge will develop a small number of initial schemes including sketches and order of magnitude cost estimates. In the second phase the collaboration will select one of these schemes for further development. This development will include scaled drawings; a detailed cost estimate that separates one-time costs – such as equipment – and recurring cost for each move operation; and a move schedule detailing the time required for each detector move. The estimated cost of this study is \$25K.

3.2 Proposed Detector Engineering

3.2.1 Introduction

As discussed above, the baseline design for the Braidwood experiment calls for two detectors each at a near and a far site. Both detector sites will be at the bottom of 175 m shafts, thus requiring the detectors to be self-contained and movable. Some preliminary engineering design (see [26] and [27]) studies have already been performed at collaborating institutions to identify the critical issues involved in constructing such a detector. Now that the experimental goals of this project have become better defined, a baseline design has been chosen. Detailed R&D work needs to be applied to fully engineer this design and establish the procedures needed for assembly, transportation, and filling of the detectors. The following sections will detail the current baseline design features and identify the engineering and research that will be needed to successfully build these detectors.

3.2.2 Baseline Detector Design

The detector systems at each site have two main components: the two-zone detector with PMTs and the (active and passive) veto system. The spherical detectors are required to be movable when completely assembled and full of oil. They first move horizontally on the surface of the earth from the assembly area up to 2 kilometers to the vertical access shafts. They must then be transported down the vertical shafts and through the tunnel into place within the veto shields. The veto system is installed inside the underground caverns and is not required to move with the detectors.

Spherical Detectors The baseline spherical detector contains 2 separate liquid zones: a central target filled with Gd-loaded scintillator and an outer buffer region containing inactive mineral oil. The two liquid regions are separated by a single acrylic sphere, greatly simplifying the assembly procedure compared to a three zone detector. In addition, the dimensions allow a total diameter of 7m for the entire detector and a radius of 2.6m for the acrylic sphere. These dimensions give a target mass of about 65 tons for each detector. Figure 11(a) shows a 2D section through the detector cavern. The drawing is to scale per the baseline dimensions of the detector.

One of the challenges of building the acrylic sphere is in fully understanding the bonding process for the pieces of acrylic that make up the sphere. Bonding tests from SNO[28] indicate that bonds of ~ 6000 psi can be achieved, but the adhesive curing reaction is exothermic. Temperature variations and shrinkage during curing can induce residual stresses in the acrylic that could cause crazing, cracking or other problems for the sphere unless properly annealed.

The liquid is contained in a spherical steel tank supported on a frame which allows the liquid-filled tank to be lifted by a crane or moved horizontally. Engineering studies (referenced below) have identified several frame designs that minimize the distortion and stress of the steel sphere. To allow assembly of the acrylic sphere inside the steel sphere, the steel sphere must have a flange at some latitude and a removable lid that allows the acrylic sphere to be lowered through the top opening. The assembled acrylic sphere is attached directly to the steel tank lid and the tank sealed before any liquid is introduced into the detector.

Mounted to the inner surface of the steel sphere are 1000 photomultiplier tubes giving a total photo-cathode coverage of 25%. For PMT assembly to the steel sphere, there may also be a man-hole access flange near the bottom of the steel sphere. Typical assembly of PMTs in spherical vessels proceeds from the top of the vessel to the bottom, with scaffolding materials removed through the lower access port.

The acrylic sphere will be supported from the removable lid of the steel sphere, and one of the major challenges of the design is to create supports for the acrylic sphere that minimize the stress on the acrylic while minimizing the optical distortion from the supports seen by the PMTs.

To control the stress and deflection of the acrylic sphere during filling of the detector, a liquid flow control system will need to be designed to match the liquid level of the mineral oil with the Gd-loaded scintillator filling the acrylic sphere.

Different designs of frames to support the steel sphere have been studied at ANL [26], FNAL [27], and Bartoszek Engineering. Figure 11(b) shows an example of one of these support structures, along with a conceptual drawing of how the acrylic sphere might be lowered into the steel sphere after attachment to the removable lid.

Veto System The Veto system has both passive and active components. Closest to the spherical detectors would be a layer of passive shielding, at least 1 meter water equivalent in thickness. Outside of the passive shielding would be a layer of active shielding to provide a muon veto.

The passive shielding needs to be a hydrogen-rich material to slow fast neutrons, and studies will have to answer the question of how much hydrogen density is enough for the purpose of this experiment, and what material satisfies the requirement at an affordable price. Ideas that have been discussed include concrete blocks and water-filled tanks with boron added as a neutron absorber. Water tanks with PMTs inside them could combine the function of active and passive shields.

There are several choices for the technology of the active shield, such as plastic scintillator

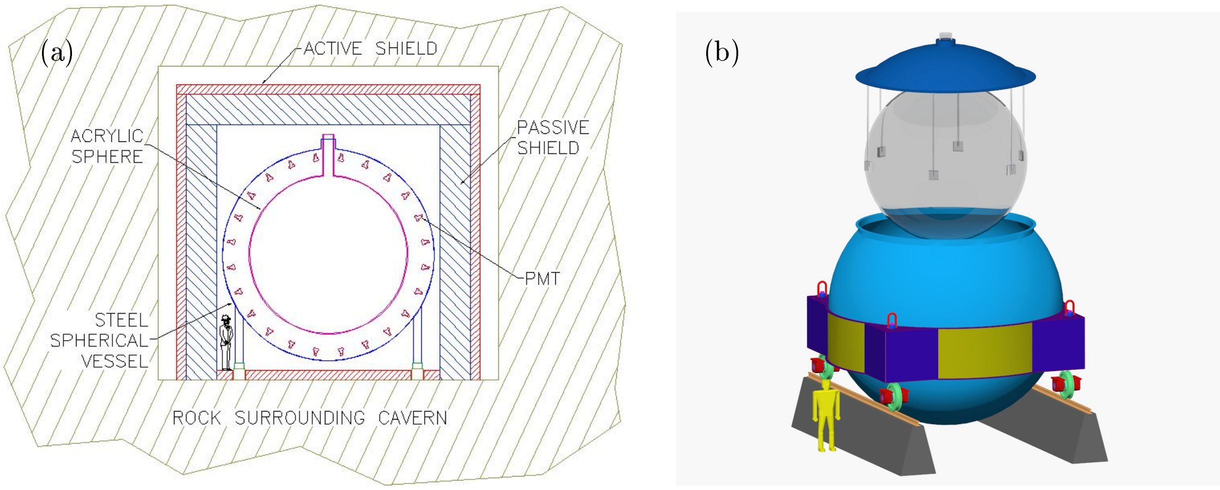

Figure 11: (a) A cross-section through a detector cavern showing the spherical detector surrounded by the veto system. The drawing is to scale. (b) Rendering showing the acrylic sphere suspended above the steel tank from the steel tank's removable lid. Also shown is one conceptual design for a support structure with the detector mounted on rails. (Figure from Bartoszek Engineering.)

paddles, wire chambers, or the liquid scintillator system described in reference [29]. Again, cost-benefit studies will have to be done to determine the technology of choice for the Braidwood experiment. To create a baseline for the cavern for civil engineering estimates, we have assumed a minimum thickness of 0.3 meters for the active shield and sufficient space around it for assembly and maintenance.

3.2.3 Baseline Detector Preliminary Cost Estimate

Table 7 below shows a very preliminary cost estimate for the detectors and veto systems. No costs are included for any detector horizontal or vertical motion systems as these technologies have not been determined. Costs have been scaled from recent MiniBooNE construction experience. A Braidwood spherical detector is one fifth of the volume of the MiniBooNE detector. Some items, such as the steel tanks, PMTs and cables, can be expected to scale as the ratio of the surface area of the Braidwood tank to the MiniBooNE tank, a factor of .34. A few sub-systems do not depend on the number of detectors built because only one item would be needed for any number of detectors.

The MiniBooNE muon tracking system covers approximately 11.8 m^2 and is based on plastic scintillator technology. The area required to be covered by a single Braidwood muon tracking system is approximately 486 square meters. The estimate for the cost of the muon tracking system comes from scaling up the MiniBooNE cost of approximately \$2100 per square meter of coverage. A different technology choice for this active veto might bring the cost down.

3.2.4 Summary of Major Detector Design Tasks for the Coming Year

Described below are some of the many aspects of the detector system that will need to be studied in the coming year in order to prepare a full engineering proposal for the Braidwood Experiment.

- *Design of Acrylic Sphere:* Work is needed to test bonding methods, develop and prototype a final design for the support structure, and perform a detailed structural analysis.
- *Design of Outer Steel Sphere:* Experience from experiments such as MiniBooNE provides a clear path to spherical tank construction; however, specification drawings are needed before steel tank vendors (e.g., Chicago Bridge and Iron and Matrix Service, Inc.) can bid on the project.
- *Calculation of Pressure Variation inside Detector:* During the movement of the detector, lateral accelerations will result in variations of the pressure distribution inside each sphere. Calculations of these variations are needed to determine the maximum pressure on the PMT's and whether a potential shock wave effect could occur. Also, the potential for damage due to a PMT imploding needs to be investigated. Studies done for MiniBooNE after the Super-Kamiokande disaster will be useful because the PMTs for Braidwood are the same size as MiniBooNE's. Studies on the possibility and consequence of a PMT implosion were also carried out by the SNO Collaboration.
- *Development of Assembly Procedure:* A procedure is needed for assembling the detector. This involves designing the fixtures, tools, and procedures for mounting the steel sphere inside its support structure, mounting the PMTs, and assembling the acrylic sphere inside the outer steel sphere.
- *Design of PMT Mounts:* The method for mounting the PMTs inside the steel sphere has to be developed in coordination with the tank specification drawings, as any features on the inside of the steel tanks may be the responsibility of the tank vendors.
- *Design of Detector Support Structure:* While preliminary work has gone into the design of an external support structure, the details of how this will fit into the restrictions imposed by the civil construction shafts and tunnels have yet to be addressed. Furthermore, the underground movement system will need to be fully designed and tested to ensure reliable operation.
- *Investigation of Materials Compatibility:* The potential of liquid scintillator to cause chemically induced defects in the acrylic is significant. Acrylic is known to work well as long as the percentage of pseudocumene is kept sufficiently low. When the final chemical composition of the liquid scintillator is defined, careful investigation will be needed to ensure that no chemically induced crazing or stresses develop. This is discussed in more detail below.
- *Scintillator Handling/Storage and Detector Filling Procedure:* By filling the inner and outer spheres simultaneously, stresses on the acrylic vessel will be greatly reduced. This will require accurate control of the fluid flow rate and the fluid levels. Also, to achieve the desired similarity between the separate detectors, it is required that the liquid in each detector be identical which can only be achieved if the liquid is mixed on site and the detectors filled at the same time. This will require the design of a large chemical storage and deployment system at the experimental site.
- *Conceptual design of the Source Positioning System:* The source positioning system allows a radioactive source to be positioned within an as-yet unspecified volume of the Gd-loaded zone. This system needs to be specified in terms of range of position, repeatability, absolute position uncertainty, and other elements characteristic of robotic positioning systems.
- *Conceptual and Preliminary Design of the Veto System:* The technology of the veto system is currently completely unspecified, for both the passive and active muon shielding. Since

this system is highly integrated with the civil construction of the underground caverns, much work is needed to put it on a par with other more developed aspects of the detectors.

3.2.5 Cost Estimate of Detector Design R&D

Table 8 gives a rough breakdown of engineering and materials and supplies (M & S) costs by subsystem for the detectors. The work represents a mixture of labor rates for Engineering, Engineering Assistants and Drafting. The M & S dollars are added to the labor dollars to obtain the value shown in the total cost column for each item.

3.3 Liquid Scintillators, Material Compatibility, and Chemical and Radioactive Contaminants

3.3.1 General Considerations

Organic liquid-scintillators (LS) have been the detection medium of choice for antineutrinos since the discovery experiment of Reines and Cowan. There are several requirements that a multi-ton LS neutrino detector must satisfy: It must (1) be chemically stable for long periods of time, (2) be optically transparent, i.e., have a large attenuation length, (3) have high light output, (4) contain ultra-low concentrations of contaminants, chemical as well as radioactive, and (5) be chemically compatible with the vessel in which it is contained.

The advantages of adding an element such as Gd to the LS (to form "Gd-LS") are:

- Only a small concentration of Gd in the liquid is required, 0.1-0.2% by weight, because some naturally occurring Gd isotopes have huge (n, γ) cross sections, $\sim 10^4$ barns.
- The energy released by the neutron capture is large, $\sim$ 8 MeV, and is distributed among several emitted γ rays, giving a distinctive angular distribution.
- The delayed coincidence time between the e^+ and n signals is shortened from $\sim$ 200 μs for n-capture in H to $\sim$ 30 μs (depending on the concentration of Gd in the LS).

However, there are several potential disadvantages to overcome:

- Trying to add inorganic salts of Gd, such as $GdCl_3$ or $Gd(NO_3)_3$, directly to the LS will not work. It is well known that the CHOOZ experiment was forced to shut down when the optical properties of its LS + $Gd(NO_3)_3$ mixture deteriorated, degrading the quality of its output signal. The observed yellow color of the CHOOZ Gd-LS was likely produced by oxidation of the organic liquid by the nitrate.
- It is not trivial to synthesize a chemical complex of Gd that will be soluble in the organic LS, which is usually a non-polar aromatic compound (i.e., contains phenyl groups and primarily C and H). This type of LS is generally immiscible with aqueous solutions.
- The Gd-LS for a neutrino experiment must be chemically stable for very long time periods, $\sim$years, as opposed to the shorter times needed for the more traditional uses of Gd-LS, for detecting high fluxes of neutrons from nuclear reactors and spallation neutron sources. "Chemical stability" means the absence of (slow) chemical reactions, such as hydrolysis and/or

polymerization, which can lead over time to cloudy suspensions in the LS or formation of gels or precipitates.

- Lanthanides, such as Gd^{3+}, often contain naturally occurring radioactive impurities, such as Th^{4+} and U^{4+} and U^{6+} (as UO_2^{2+}). Purification steps will have to be developed and used to reduce these radioactive species to concentrations $\sim 10^{-12}$ g/g. Concentrations of other non-radioactive chemical species that can adversely affect the optical properties of the Gd-LS will also have to be strictly controlled.
- Most of the envisaged purification steps will have to be applied before and during the synthesis of the Gd-LS. Most chemical separation schemes that would be used after the Gd-LS has been put into the detector vessel would be unsuitable because they would likely remove some of the Gd as well as the other inorganic impurities. Even vacuum techniques for removing Rn from the Gd-LS could cause problems by changing the concentrations of the volatile organic liquid components in the LS.
- The chemical compatibility of the organic LS with the material of the detector vessel is another important factor to study. Acrylic is known from SNO R&D to be attacked by many chemical liquids. Nylon, as used in Borexino and in KamLAND, is known to be resistant to some LS, such as PC and mineral oil. Another aspect of this problem that should be realized is that chemical attack and/or leaching of the vessel by the LS could introduce unwanted impurities, organic as well as inorganic, from the vessel into the liquid and adversely affect the LS properties.
- The requirement of achieving a 1% precision in the Braidwood Experiment magnifies the above challenges inherent in preparing the Gd-LS. For example, the concentrations not only of Gd but also of LS (i.e., the concentrations of target H atoms for the antineutrino capture), must be identical in the near and far detectors. Special care will thus have to be given to the batch-wise preparation of the Gd-LS and to the chemical quantitative analyses of these batches.

3.3.2 Research to date at BNL on metal-loaded LS

Since 2000, the Solar-Neutrino/Nuclear-Chemistry Group in the BNL Chemistry Department has been involved in R&D of chemical techniques for loading metallic elements, such as In^{3+} and Yb^{3+}, up to concentrations of several percent by weight, into organic LS (in collaboration with R. S. Raghavan of Bell Labs). This research, in a project called LENS-Sol, has as its main goal the development of a detector capable of observing low-energy neutrinos from the solar pp and ^{7}Be branches, via neutrino capture on the In (with a Q-value of 0.114 MeV). The principle of the chemistry is straightforward, namely to prepare an organometallic complex of In that is soluble in the LS. But the execution has been difficult, with many problems to solve and details to master.

Several organic complexing agents come to mind, for example (i) carboxylic acids (RCOOH) that can be neutralized with inorganic bases such as NH_3 to form metal carboxylates, (ii) organic phosphorus-oxygen compounds, such as organic phosphates or phosphine oxides, that can complex neutral inorganic species such as $InCl_3$, and (iii) organic diketones, such as acetyl acetonate. Compounds from groups (i) and (ii) were selected as candidates for testing proposed chemical procedures at BNL. Much of their organometallic chemistry has already been developed in the fields of separations chemistry and chemical treatment of the nuclear fuel cycle.

After extensive laboratory R&D, procedures have been worked out for the purification of the chemical components and synthesis of the metal-LS by solvent-solvent extraction. Much of the focus has been on the carboxylic acids, because they are produced in bulk by the chemical industry and have lower cost and ease of chemical disposal, as compared with the phosphorus-containing compounds. Several carboxylic acids, with side chains containing from 1-8 carbons, have been studied. The best candidate found to date is methylvaleric acid, MVA. Reproducible results with MVA have been found for samples of In-LS, where In concentrations are in the 5-10% range and the organic solvent, PC, is the LS.

Many methods, instrumental and chemical, have been developed at BNL to analyze the resulting In-LS samples. Among these are (1) measurement of the attenuation length both by UV-Visible absorption spectrophotometry with 10-cm optical cells and by a dual-beam, long-pathlength (>1 meter) blue laser system; (2) measurement of the light yield, S%, relative to the pure PC LS; and several chemical determinations of the In-LS, such as of the concentrations (3) of the In^{3+} by a colorimetric method, (4) of the total RCOOH by acid-base titrations, (5) of the uncomplexed RCOOH by IR spectroscopy, (6) of the H_2O by Karl-Fischer titrations, (7) of the NH_4^+ and Cl^- by electrochemistry, and (8) of different In species in the organic liquid by IR spectroscopy.

Early in 2004, because of the developing interest of the BNL Group in θ_{13} experiments, the procedures that had been developed for In-LS were successfully applied to the preparation of some initial samples of Gd-LS. Samples of $\sim$3% Gd-LS in PC were made and then diluted to Gd concentrations, $\sim$1%, 0.5%, and 0.1%. Figure 12 (a) shows the 10-cm absorption spectra and the absorbance values, R at 430 nm, for these samples. These R-values translate into 1/e attenuation lengths of $\sim$5 to 15 meters. Figure 12 (b) shows the Compton-scattering light-yield curves, produced by an external source of ^{137}Cs irradiating these samples. The 0.1% Gd-LS has a light yield relative to pure PC of 94%. The properties of these samples are also being monitored over time, to search for any degradation of the Gd-LS. Over a period of the first few months, the properties of these samples have not changed.

Some samples of commercially available Gd-LS were obtained (Bicron BC-521 with 1% Gd in PC and BC-525 with 0.5% Gd in mineral oil) and compared with the BNL samples. The light yields of the respective BNL and Bicron were found to be comparable, but the attenuation lengths of the BNL Gd-LS were more than two times larger than the Bicron samples, probably reflecting the care put into the BNL pre-synthesis purification steps.

3.3.3 Future Research at BNL on Gd-LS

These initial results on Gd-LS are very encouraging for the Braidwood Experiment and merit further R&D. The BNL Group plans to increase its efforts in the short term.

One major focus will be to optimize, simplify and finalize the chemical procedures to synthesize the Gd-LS. Issues of chemical purifications and of the control and assay of radioactive impurities will have to be addressed. There are two approaches to making batches of the Gd-LS: (a) preparing each batch at the desired final Gd concentration, 0.1-0.2%, or (b) preparing more concentrated batches, at least 1-2% Gd, and then diluting with the organic LS to the desired concentration. The two approaches are not identical, with regard to possible long-term effects such as hydrolysis, polymerization, and effects on the optical properties of the final Gd-LS. Approach (b), however, may simplify preparation of larger volumes of Gd-LS.

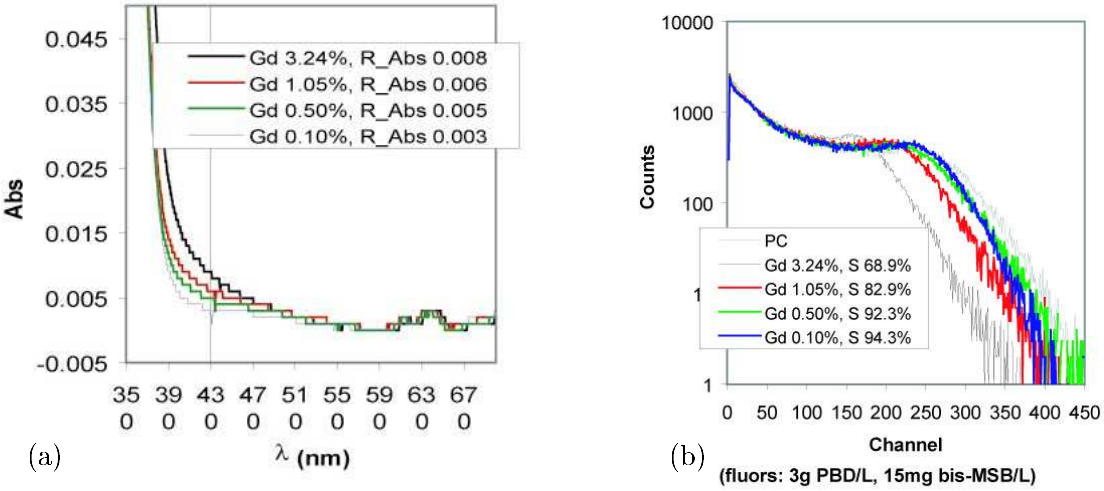

Figure 12: (a) Absorption spectra of BNL Gd-LS, and (b) light yields of BNL Gd-LS.

In the long term, consideration will have to be given to designing and building chemical systems that (i) are closed to prevent ingress of air, which can degrade the LS, and (ii) are automated to replace many of the procedures that are currently done in the laboratory by hand. After that, one will have to increase the scale of the syntheses, from the present 0.5-1 liter per batch to at least 5-10 liters per batch. A goal has been set in the collaboration of accumulating ~200 liters for prototype tests.

As the BNL R&D continues, all of the analytical methods that have been described in Section 3.3.2 for In-LS will be used to determine the chemical and physical properties of the Gd-LS. The timing characteristics of the light signals produced by the Gd-LS may also be investigated, such as the pulse widths and decay times.

Another important issue to study is the compatibility of the detector vessel material with the Gd-LS. In addition to PC, other organic liquid scintillators are known, such as phenyl cyclohexane (PCH) and various types of mineral oil. It has been reported that a mixture of 20% PC - 80% mineral oil, and possibly even 40% PC - 60% mineral oil, will not attack acrylic. These claims will have to be verified.

Once the project gets into planning for the full-scale experiment, or possibly for an intermediate-size prototype, the volumes of liquids being produced will be on the level of tons. Industrial cooperation will likely be required. At that juncture, it will be very important to have a quality control program already developed and in place in the collaboration so as to verify the quality of the materials that will be supplied by the vendors, e.g., pure solvents, starting materials for the Gd-LS synthesis, or even commercially manufactured Gd-LS.

There are many topics to investigate. The BNL Group is relatively small and may have more ambitious plans than it can accomplish in a reasonable time span. It intends to cooperate with other groups in the collaboration to leverage its efforts. It will also provide samples of Gd-LS for measurements that will be done at other institutions and/or participate in exchanging samples between different institutions ("round robin") to get independent measurements of key quantities, such as attenuation lengths and light yields.

The BNL Group is funded by DOE's Office of Nuclear Physics, for its ongoing research in SNO and for exploring new research directions, such as LENS-Sol and the Braidwood Experiment. While no additional funds for scientific support are being requested for BNL, this proposal does contain a request for the cost of purchases of chemicals and materials to be used in R&D on the synthesis of the Gd-LS. That amount for the first year is $28,000.

4 Elastic Scattering Measurements at Reactor Experiments

The availability of a high statistics, high precision reactor neutrino experiment provides an ideal environment to search for new exotic physics. This measurement is unique to Braidwood, because this is the only site which offers sufficient overburden as well as the required proximity to the reactors. In particular, one can use neutrino-electron scattering to make precision tests of what is predicted by the Standard Model. Neutrino-electron scattering is sensitive to one of the most fundamental parameters in the Standard Model of particle interactions, the weak mixing angle. Deviations from theoretical prediction would be evidence of new physics processes at work.

The differential cross-section for $\bar{\nu}_e + e^- \to \bar{\nu}_e + e^-$ scattering is given by the following expression [30]:

$$\frac{d\sigma}{dT} = \frac{G_F^2 m_e}{2\pi}[(g_V + g_A)^2 + (g_V - g_A)^2(1 - \frac{T}{E_\nu})^2 + (g_A^2 - g_V^2)\frac{m_e T}{E_\nu^2}] + \frac{\pi\alpha^2\mu_\nu^2}{m_e^2}\frac{(1 - T/E_\nu)}{T} \qquad (1)$$

where E_ν is the incident $\bar{\nu}_e$ energy, T is the electron recoil kinetic energy, and g_V and g_A are the vector and axial vector coupling constants.

The electron scattering cross-section allows a direct measurement of the weak mixing angle θ_W, which is related to g_V. As such a process is purely leptonic, it is void of uncertainties associated with nuclear structure or strong interactions. A high precision future measurement of the weak mixing angle is motivated, in part, by the result reported by the NuTeV experiment, which measures a 3σ deviation from Standard Model predictions [31]. Various exotic models to explain the measurement have been put forward, and those which best explain the result require a follow-up experiment which probes the neutral weak couplings specifically using neutrinos. The proposed measurement is also interesting as an additional precision study at $Q^2 = 4 \times 10^{-6}$ GeV^2. The two existing low Q^2 measurements are from atomic parity violation [32], and Moller scattering [33]. A careful, controlled measurement of neutrino-elastic scattering should provide a measurement of the weak mixing angle at the level of 1%.

The technique of using reactor neutrinos to measure the weak mixing angle has been pioneered by Reines, Gurr, and Sobel [34]. The weak mixing angle measurement comes mainly from tagging electrons that possess an energy greater than 3 MeV. Above this energy threshold, many of the environmental backgrounds are reduced or removed entirely. In order to make a precision measurement, the incoming neutrino flux has to be known to better than 0.5%. Current uncertainties in nuclear fuel burning limit one's knowledge of the neutrino flux and spectrum to no better than 2%. Thus, it is necessary to use inverse beta decay events ($\bar{\nu}_e + p \to e^+ n$) as a normalization constraint. These events can be tagged by the subsequent neutron capture on Gd. The uncertainty on the cross section for inverse beta decay of low energy neutrinos is only 0.2%, making it an ideal process by which to normalize electron scattering events.

To reduce the uncertainties associated with neutrino electron scattering, careful control must be placed on the backgrounds and systematics associated with counting the number of electrons and their subsequent recoil energies. Further details regarding background rejection and error reduction techniques can be found in Reference [35]. A total uncertainty of 1.3% is, in principle, achievable with sufficient flux, adequate overburden, and a careful calibration program. We believe such a measurement will greatly complement a θ_{13} measurement program at reactor experiments.

In addition to being a direct probe to the weak mixing angle, neutrino-electron scattering is also sensitive to other exotic physics. More notably, the differential cross-section $\bar{\nu}_e + e^- \rightarrow \bar{\nu}_e + e^-$ depends also on the neutrino magnetic moment, μ_ν. The Standard Model prediction for the neutrino magnetic moment is very small, $\mu_\nu \sim 10^{-19}\mu_B$. Thus, a positive measurement of μ_ν beyond this prediction would be a strong indication of new physics. The current limit from reactor experiments on the neutrino magnetic moment is less than $1.3 \times 10^{-10}\mu_B$ at the 90% confidence level [36]. Reactor experiments may be able to probe at this level of sensitivity or greater.

The precision measurement of the antineutrino-electron elastic scattering cross section has more stringent requirements on certain detector issues, such as contamination levels and energy calibration, than the oscillation measurement. R&D on these issues will proceed over the next two years, and modest funding for this is being requested separately as a part of base grant proposals. Here we provide some initial information on these studies.

With respect to contamination, the issue is U and Th, since the measurement is restricted to the 3 to 5 MeV range. Purification of scintillator to the requisite level is well understood from KamLAND and Borexino experience. However, the question of U and Th contaminants in the rare earth metal Gd, used as a dopant, remains open. For a similar rare earth metal, Yb, a satisfactory contamination level of 10^{-12} has been achieved, leading us to believe that with R&D this can also be attained with Gd using similar methods. Even less contamination is desirable and so work will continue to aim for purities beyond 10^{-12}.

On energy reconstruction, it is desirable to find a method which can calibrate the detector in the energy window for both β^+ and β^- events. Possible sources and methods for deployment are under consideration. The plan is to bench test these ideas over the next year. The ambitious goal is 0.3% (for comparison, SNO calibrated their detector energy scale to 1%).

Other issues are also under study. One example is the fiducial volume error, which is greatly reduced by the fact that we are measuring elastics scattering with respect to the inverse beta decay rate. Another is spallation, which may lead us to narrow our energy window to 3.5 to 5 MeV, which sacrifices statistics for better identification of the spallation, as well as reducing the background from contamination.

Table 7: Preliminary cost estimate for one spherical detector and its associated veto system for the Braidwood Reactor Neutrino Project, and total cost for four detectors.

Description	Est. Cost (thousands of dollars)
Spherical Detectors	
Steel tank	340
Acrylic vessel	500
Oil	89
Gd-loaded Scintillator	640
Oil plumbing system	100
Temp regulation system, N2 purge	40
PMTs	870
PMT supports	100
Cable system	7
Tank support system	50
Detector electronics	150
DAQ	50
Assembly Labor	65
Radioactive Source Scanning System	100
Muon System	1,100
Subtotal per Detector and Veto	4,201
Contingency (30%)	1,260
Total for one Detector System with cont.	5,461
Total for four Detector Systems with cont.	21,844
Items independent of number of detectors	Est. Cost
Attenuation Length Tester	29
Storage Tank Farm on Site	750
Subtotal of above items	779
Contingency (30%)	234
Subtotal of above items with contingency	1,013
Overall Total with contingency	22,857

Table 8: Estimate of detector engineering and M & S costs for the Braidwood Experiment planned for coming year.

Task Name	M & S	Work (hours)	Total Cost (thousands of dollars)
Spherical Detectors			
Steel tanks	$0	160	14
Acrylic vessels	$0	378	35
Oil	$10,000	168	27
Oil plumbing system	$0	364	35
PMT system	$0	200	19
Cable system	$0	160	9
Tank support system	$0	320	29
Detector electronics	$0	104	10
Radioactive source scanning system	$0	616	56
Muon System			
Passive shielding	$0	498	44
Muon tracking system	$0	538	48
Subtotal	$10,000	3,678	326
Contingency (25%)	$0	0	82
Total	$10,000	3,678	408

References

[1] S. L. Chen, M. Frigerio and E. Ma, arXiv:hep-ph/0404084; I. Dorsner and A. Y. Smirnov, arXiv:hep-ph/0403305; S. Antusch and S. F. King, Phys. Lett. B **591**, 104 (2004) [arXiv:hep-ph/0403053].

[2] P. Huber, M. Lindner, M. Rolinec, T. Schwetz and W. Winter, the arXiv:hep-ph/0403068.

[3] P. Huber, M. Lindner, T. Schwetz, and W. Winter. Nucl. Phys., **B**665 487, 2003. hep-ph/0303232.

[4] H. Minakata, H. Sugiyama, O. Yasuda, K. Inoue and F. Suekane, Phys. Rev. D **68**, 033017 (2003) [arXiv:hep-ph/0211111].

[5] H. Minakata, M. Sonoyama and H. Sugiyama, experiments arXiv:hep-ph/0406073.

[6] F. Ardellier *et al.*, "Letter of intent for double-CHOOZ: A search for the mixing angle theta(13)," arXiv:hep-ex/0405032.

[7] K. B. McConnel and M. H. Shaevitz, arXiv:hep-ex/0409028.

[8] M. Apollonio *et al.* Phys. Lett., **B**420 397–404, 1998. hep-ex/9711002.

[9] F. Boehm *et al.* Phys. Rev., **D**62 072002, 2000. hep-ex/0003022.

[10] VSPLAT Experiment, http://www.nevis.columbia.edu/c̃onrad/vsplat.html.

[11] M. Hurwitz and J. Pilcher, "Simulation of Cosmic Ray Muon Flux at Shallow Depths Underground", http://braidwood.uchicago.edu/text/Muon.pdf (July, 2004).

[12] V.A. Kudryavtsev, N.J.C. Spponer, J.E. McMillan, Nucl. Instrum. Meth. **A505**, 638 (2003).

[13] T.K. Gaisser, *Cosmic Rays and Particle Physics*, Cambridge University Press, 1990.

[14] M. Apollonio et al. (CHOOZ collaboration), Eur. Phys. J. **C27**, 331 (2003).

[15] Y.-F. Wang, *et al.* Phys. Rev. **D** 64, 013012 (2001).

[16] T. Araki, et al. (KAMLAND collaboration), hep-ex/0406035 (June, 2004).

[17] G. Horton-Smith, "Quashing Backgrounds", 2nd International Workshop on Future Reactor Neutrino Experiments, Oct. 10, 2003, Munich, Germany, www1.physik.tu-muenchen.de/lehrstuehle/T30d/events/reactor03/pages/transparencies/horton-smith.pdf.

[18] J. Pilcher and M. Hurwitz, http://braidwood.uchicago.edu, 2005.

[19] Y-F Wang et al., hep-ex/0101049.

[20] N.V. Mokhov, et al., Fermilab-FN-628, 1995.

[21] Geant4 Collaboration, NIM A506(2003)250.

[22] Y.-F. Wang, *et al.* Phys. Rev. **D** 62, 013012 (2000).

[23] Exelon Nuclear, *Byron & Braidwood Stations Updated Final Safety Analysis Report*, December 2002.

[24] Jack de la Vergne, *Hard Rock Miners' Handbook*, MaIntosh Engineering Inc., 2003.

[25] Gary S. Brierley and David J. Hatem, editors, *Design-Build Subsurface Projects*, Zeni House Books, 2002.

[26] http://gate.hep.anl.gov/vjg/Reactor-Baseline1.doc

[27] A Structure Analysis For the Sphere Tank Support Used as the Reactor Neutrino Detector In the Braidwood Experiment, Ang Lee and Hans Jostlein, September 1st, 2004

[28] SNO-STR-91-3 Acrylic Mechanical Bond Tests

[29] J. J. Napolitano et al, Construction and Performance of a Large Area Liquid Scintillator Cosmic Ray Anticoincidence Detector, Nucl. Instr. and Meth. 274 (1989) 152-164

[30] D. Y. Bardin, S. M. Bilenky and B. Pontecorvo, Phys. Lett. B **32**, 68 (1970).

[31] G. P. Zeller *et al.*, Phys. Rev. Lett. **88**, 091802 (2002) [Erratum-ibid. **90**, 239902 (2003)]

[32] S. C. Bennett and Carl E. Wieman, Phys. Rev. Lett. **82**, 2484 (1999).

[33] P. L. Anthony *et al.* [SLAC E158 Collaboration], Phys. Rev. Lett. **92**, 181602 (2004)

[34] F. Reines, H. S. Gurr, and H. W. Sobel, Phys. Rev. Lett. **37**, 315 (1976).

[35] J. M. Conrad, J. M. Link and M. H. Shaevitz, arXiv:hep-ex/0403048.

[36] H. T. Wong, arXiv:hep-ex/0409003.